Chapter 8

RF System

In this chapter we describe the RF hardware components for KEKB. RF stations will be located in three straight sections, called Oho, Fuji, and Nikko (see, Figure 8.1). It has been recommended from simulations regarding the ring dynamic aperture that the RF cavities for the LER should be located at the Fuji straight section which is opposite to the Tsukuba interaction region. The RF stations for the HER will be located in the Oho and Nikko straight sections.

A block diagram of each RF unit for the ARES cavities is shown in Figure 8.2. A 508 MHz 1MW CW klystron will feed the power to two ARES normal-conducting cavities or one superconducting cavity. Best efforts will be made to use the existing infrastructures and facilities in the TRISTAN accelerator to minimize the construction cost. In particular, the existing klystrons, together with the power supply systems and the cooling systems for the klystrons, wave guide components, magic tees and circulators will be re-used in KEKB. In addition, a 6kW large refrigerator system, which has been operated for the superconducting cavities in TRISTAN, can be re-used.

Extensive R&D work is in progress on both the ARES and the superconducting cavity. Coupled-bunch instabilities arising from the accelerating mode and the higher order modes are expected to be sufficiently suppressed, as discussed in chapter 4.

In the following, detailed descriptions of the ARES and the superconducting cavity are given in section 8.1 and section 8.2, respectively. Section 8.3 treats the issues related to the RF low level system, including the effect of a bunch gap and the R&D work of an RF cavity feedback system. Section 8.4 discusses a crab cavity for the crab crossing, which will be implemented as a fall-back solution to the problems encountered with the finite angle crossing scheme.

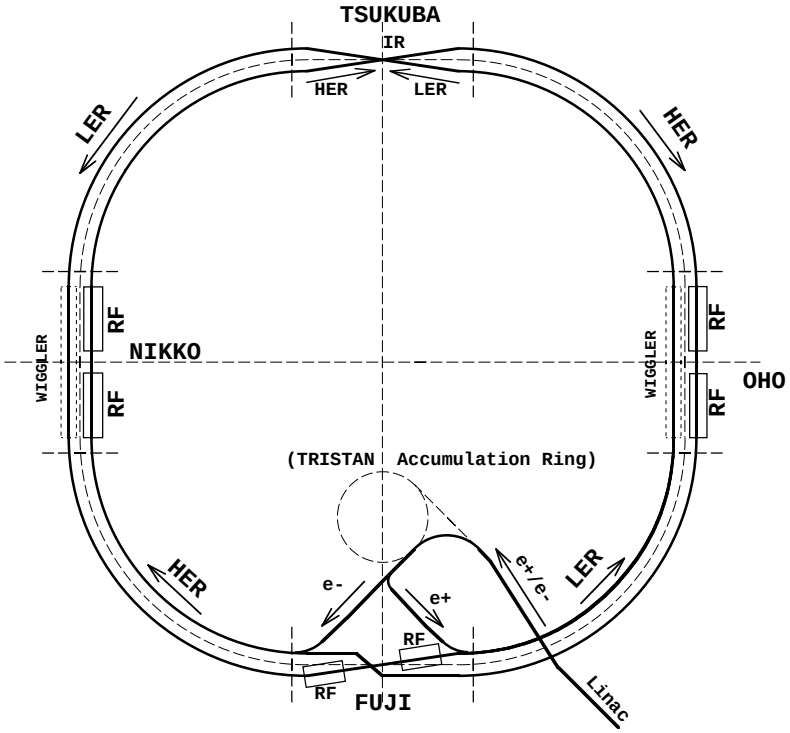

Figure 8.1: Schematic plan view layout of KEKB.

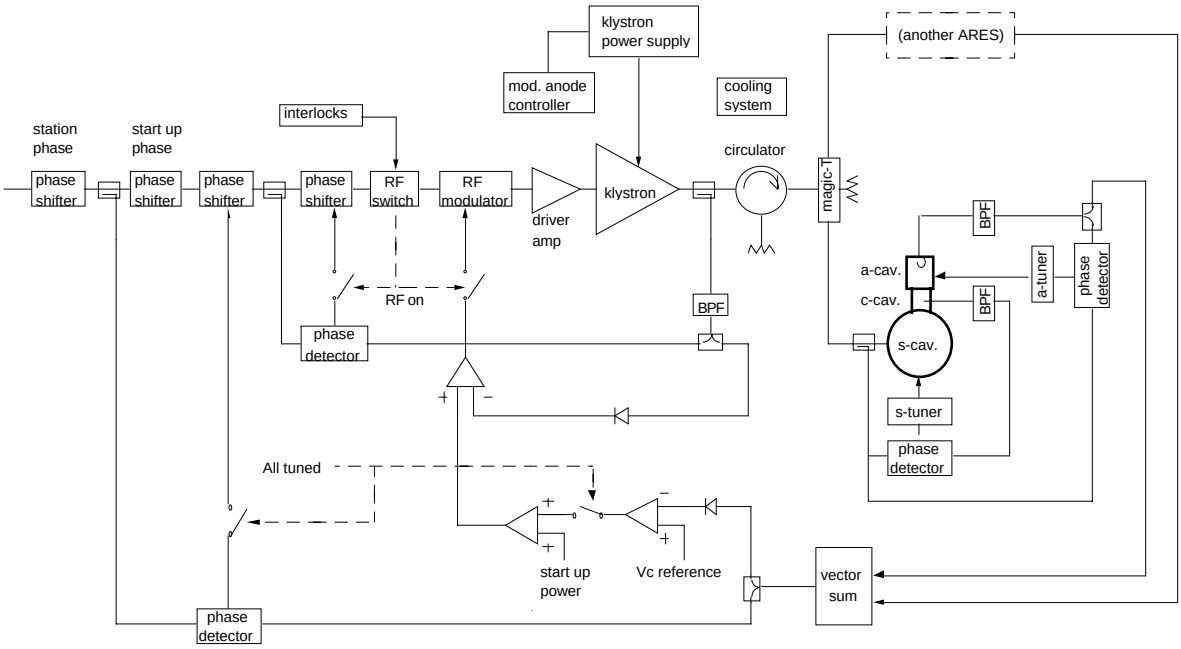

Figure 8.2: Block diagram of one RF unit with the ARES cavities.

8.1 Normal Conducting Cavity

8.1.1 ARES scheme

The accelerator resonantly coupled with an energy storage (ARES) [1] is expected to break through the difficulties concerning the coupled-bunch instabilities arising from the accelerating mode. As shown in Figure 8.3, it has an energy storage cavity coupled with an accelerating cavity via a coupling cavity. As discussed in chapter 4, owing to a large stored energy in the storage cavity, the detuning frequency is reduced and the instability is sufficiently suppressed.

The reason why the coupling cavity is implemented is explained in the following. The original scheme of employing an energy storage cavity was proposed by T. Shintake [2], where no coupling cavity is used. However, this scheme has a couple of problems. The first one is an instability arising from a parasitic mode which exists near the accelerating mode. When the accelerating cavity is coupled with the energy storage cavity, the accelerating mode splits into two eigenmodes. One is called the 0

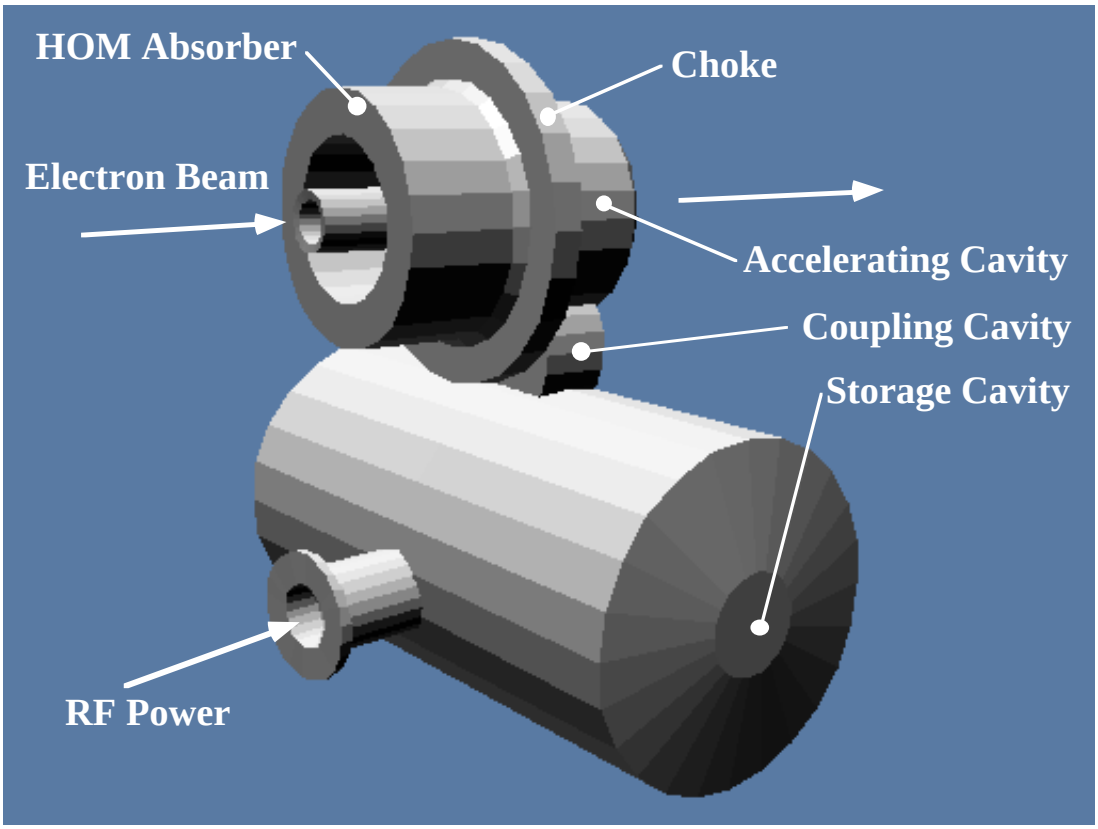

Figure 8.3: Schematic view of ARES.

mode, and the other the π mode, according to the phase difference between the two cavities. For example, the 0 mode becomes the parasitic mode when the π mode is employed for beam acceleration. The coupling impedance of the parasitic mode has the same order of magnitude as that of the accelerating mode. Therefore, the growth rate of the instability will be as large as that due to the accelerating mode of a conventional single-cell cavity. The second problem is that the field amplitude and phase of the π mode is unstable against heavy beam loading.

By employing a coupling cavity in the ARES, these difficulties in using an energy storage cavity can be successfully solved. Since the ARES has three resonators, the accelerating mode splits into three eigenmodes: the 0 mode, the $\pi/2$ mode, and the π mode. The ARES scheme has the following advantages over the former coupled-cavity system where an accelerating cavity is directly coupled with a storage cavity. First, the operating mode of the ARES is the $\pi/2$ mode, which has excellent field stability against the heavy beam loading. Second, the ratio of the stored energy in the storage cavity relative to that in the accelerating cavity can be adjusted by changing the relative strength of the coupling factor between the storage and coupling cavities vs. that between the accelerating and coupling cavities. Third, the $\pi/2$ mode has almost no field excitation in the coupling cavity. Therefore, the two parasitic modes (the 0 and π modes) can be selectively damped by installing a coupler in the coupling cavity, while the $\pi/2$ mode is not affected. Finally, the 0 and π modes are located nearly symmetrically with respect to the $\pi/2$ mode. Therefore, the contributions of the impedance of the damped parasitic modes to the instability are expected to be counter-balanced to some extent.

The basic design of the ARES was carried out on the basis of a three-dimensional analysis of the RF properties [3] by using the computer code MAFIA.

Storage Cavity

As the storage cavity, we chose a cylindrical cavity operating in the TE015 mode, which is the same mode employed in the SLED [4]. For an RF frequency of 509 MHz, the dimensions of the storage cavity are about 1100 mm in diameter and about 2000 mm in axial length. Assuming the standard value of copper conductivity, the Q value of the TE015 mode is estimated to be 2.6×10^5, which is sufficiently high to store a large amount of the field energy with a low wall power dissipation.

Since the storage cavity has many parasitic modes in the vicinity of the TE015 mode, the perturbation of opening a slot to the coupling cavity easily mixes parasitic modes into the TE015 mode. Mixing with a low-Q mode would deteriorate the high Q value of the operating mode. Therefore, careful fine tuning of the cavity dimensions

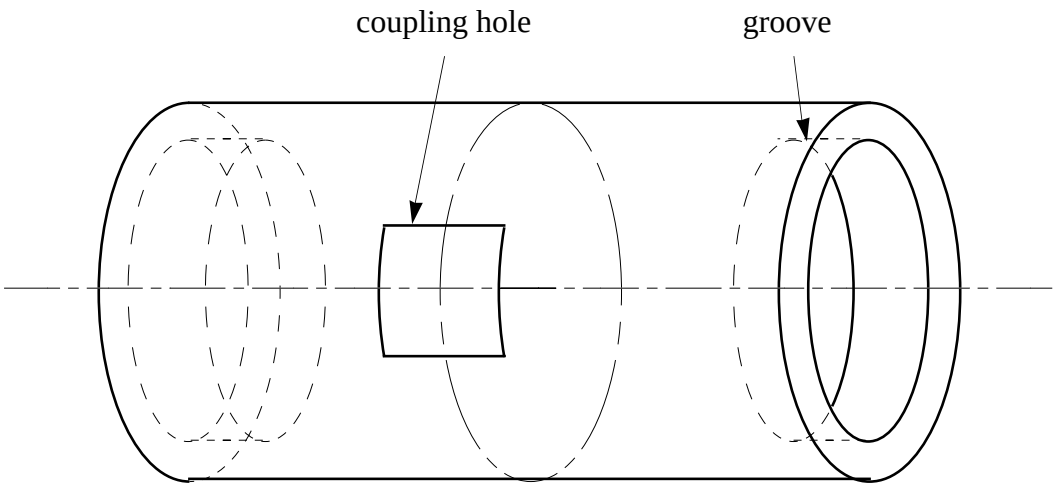

Figure 8.4: Schematic view of the storage cavity.

is required to prevent parasitic mode mixing.

Figure 8.4 shows a schematic drawing of the storage cavity with a coupling slot arranged to keep the mirror symmetry with respect to the mid-plane between the two end plates. The circumferences of both end plates are grooved in order to remove the degeneracy of the TE015 and TM115 modes. This method was first applied in the SLED cavities [4]. A groove depth of 80 mm gives a sufficient mode separation of 16 MHz.

According to a precise study [3] concerning the perturbative effect of the coupling slot, the TE015 mode should be kept away from the TEmnp(p=odd) and TMmnp($m >$ 0, p=odd) modes to minimize the parasitic mode mixing. Figure 8.5 shows a mode diagram of a cylindrical cavity without grooves at the end plates. The ratio of the radius to the axial length was carefully chosen to obtain the best location of the TE015 mode among the harmful parasitic modes. The frequency shift of each harmful parasitic mode due to the grooves must also be taken into account. For example, the frequency of the TM213 mode, which is close to the TE015 mode in the mode diagram, is actually lowered by 10 MHz due to the grooves.

Basic RF Design of the ARES

In the RF design of the ARES, we started with the most simple case, where a cylindrical accelerating cavity is coupled with the storage cavity via a cylindrical coupling cavity. Figure 8.6 shows a schematic view of the structure. The ratio of the axial length of the coupling cavity to that of the accelerating cavity was chosen to be just half.

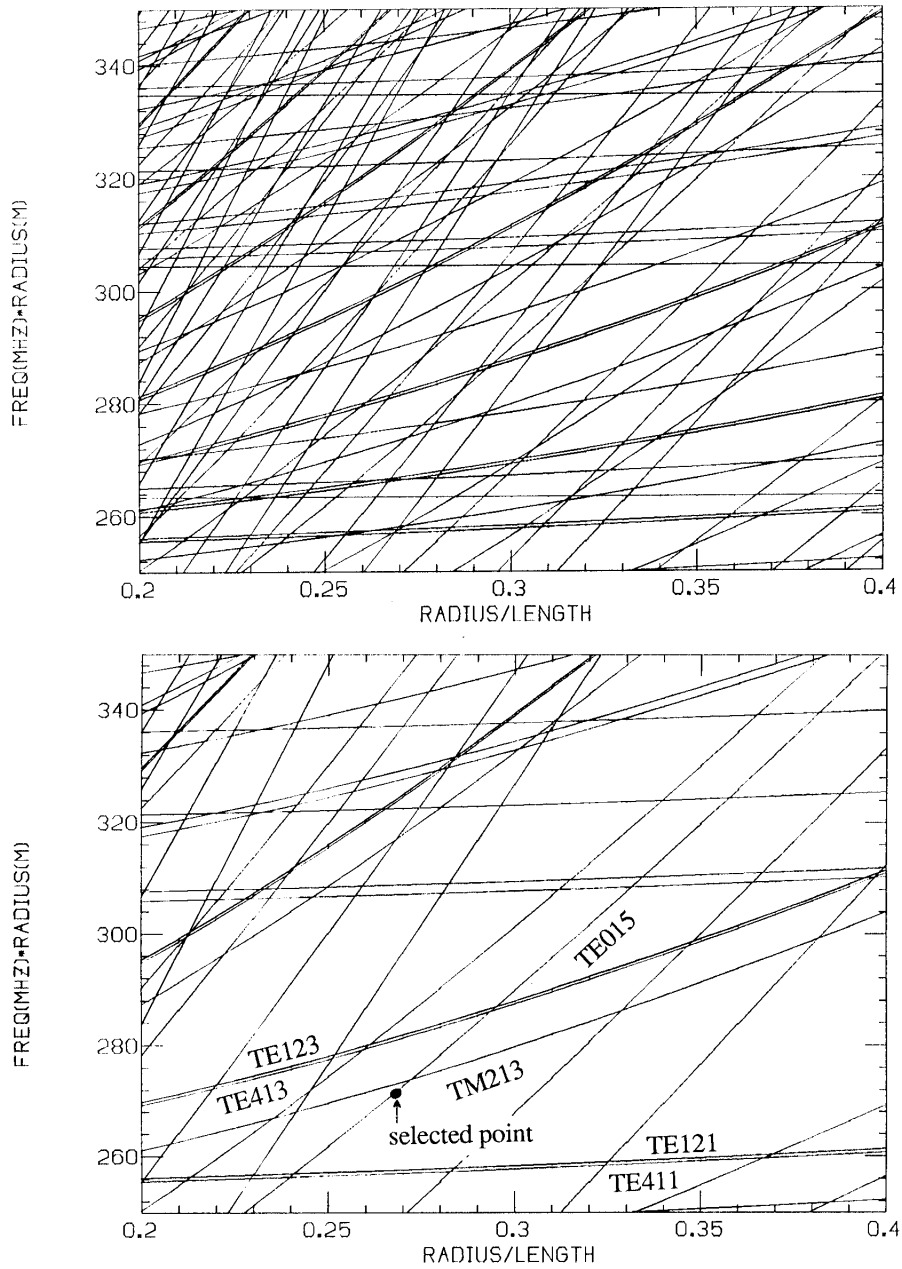

Figure 8.5: Mode diagram in a pillbox cavity. (upper) all TE and TM modes, and (lower) TEmnp (p=odd) and TMmnp ($m > 0$, p=odd) modes.

Iterative optimization of the structure is performed [3] using MAFIA until the following requirements are satisfied:

1. Each cavity should be tuned to the same frequency of 508 MHz under the $\pi/2$-mode boundary condition. This assures that almost no field is excited in the coupling cavity for the operating mode.

2. The stored energy in the storage cavity should be larger than that in the accelerating cavity by factor 10. This reduces the detuning frequency under beam loading by an order of magnitude.

3. The 0 and π modes should be nearly symmetrically located with respect to the $\pi/2$ mode. This assures counter-balancing the contributions of the 0- and π-mode impedance to the coupled-bunch instability.

Each cavity frequency was tuned by changing its radius. The ratio of stored energies was adjusted by changing the ratio of the coupling factor k_s between the storage and coupling cavities to k_a between the accelerating and coupling cavities.

The optimized dimensions of the ARES are listed in Table 8.1. The RF properties of the operating mode are listed in Table 8.2, together with those of the parasitic modes. Figure 8.7 shows the electromagnetic fields of the $\pi/2$ mode. As can be seen from the field pattern, the mixing of parasitic modes into the TE015 mode is successfully suppressed, and almost no field is excited in the coupling cavity. Most of the field energy is stored in the storage cavity in the form of the low-loss TE015 mode. The R/Q value of the total ARES system is reduced by an order of magnitude compared to that of a conventional single-cell copper cavity. This means that the required detuning frequency is also reduced by the same magnitude. On the other hand, the Q value of the system is increased by factor 5, compared to a copper cavity. Therefore, the shunt impedance of the ARES is kept at a reasonable level. According to the operating RF parameters discussed in chapter 4, the growth time of the instability due to the accelerating mode is longer than 30 ms (LER) and than 100 ms (HER), which is sufficiently long compared with the radiation damping time.

Figure 8.8 shows the field patterns of the parasitic modes in the vicinity of the operating mode, including the 0 mode at 501.7 MHz and the π mode at 512.8 MHz. Since the coupling cavity is excited for all parasitic modes, these can be damped by extracting the field energy through a coupler attached to the coupling cavity. The growth time of the instability due to the damped parasitic modes has been calculated [3] using the R/Q values in Table 8.2. Figure 8.9 shows the fastest growth time as a function of the loaded Q value. If the loaded Q values of the parasitic modes are

Table 8.1: Dimensions of the optimized shape.

cavities	accelerating	coupling	storage
radius (mm)	224.0	213.5	535.2
length (mm)	260.0	130.0	1989.4
coupling holes			
location	between a- and c-		between s- and c-
length (mm)	130.0		200.0
width (mm)	180.0		130.0
distance (mm)	0.0		0.0

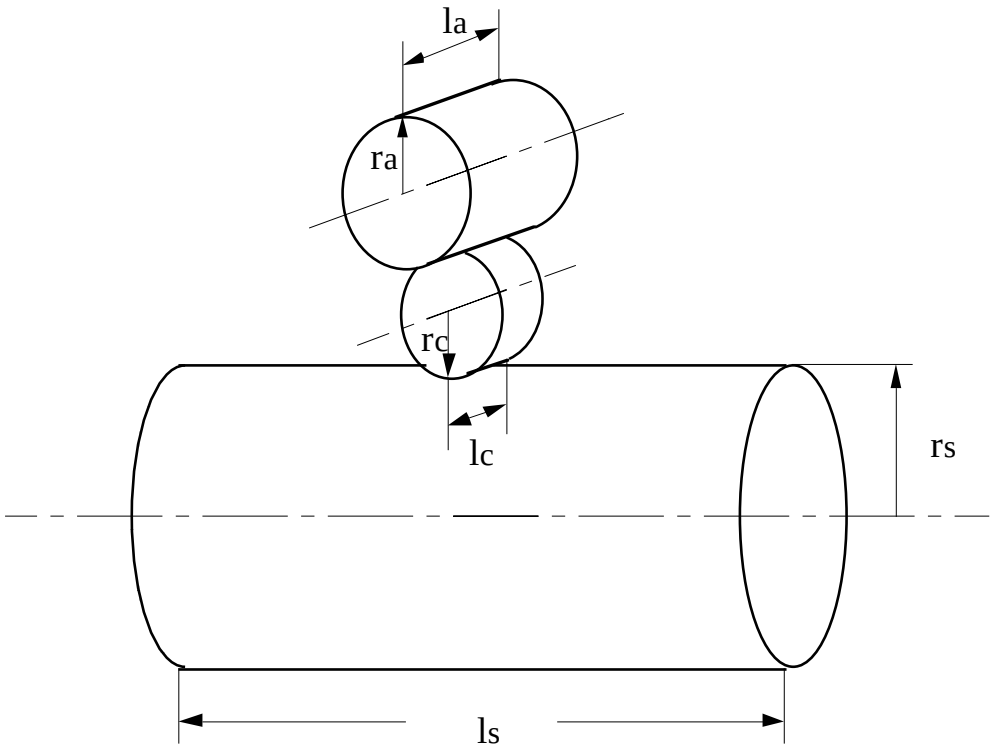

Figure 8.6: Schematic view of the three-cavity system.

Table 8.2: Properties of the optimized design.

operating mode (TE015, $\pi/2$)				
	frequency	(MHz)	508	
	$Q_{\rm total}$		1.8×10^5	
	$R/Q_{\rm total}$	(Ω)	13.9	
	ka		5.6 %	
	ks		1.0 %	
parasitic modes				
TEmnp (p=odd), TMmnp (m>0, p=odd)				
	frequency (MHz)	mode in s-cav.	$R/Q_{\rm total}$ (Ω)	
	474.0	TE411	0.12	
	479.5	TE121	0.04	
	491.2	TM115	0.02	
	499.1	TM213	0.75	
	501.7	TE413/TM213	105.	(0 mode)
	512.8	TE413	71.8	(π mode)
	518.3	TE315	1.04	
	521.0	TE413	16.4	
TEmnp (p=even), TMmnp (p=even)				
	472.3	TM212		
	473.4	TE116		
	475.0	TE314		
	492.0	TE412		
	497.2	TE122		
	516.4	TE216/TM214		
	537.3	TE216/TM214		
	537.7	TM116		
TM0np				
	484.3	TM016		
	501.0	TM022		
	522.4	TM023		

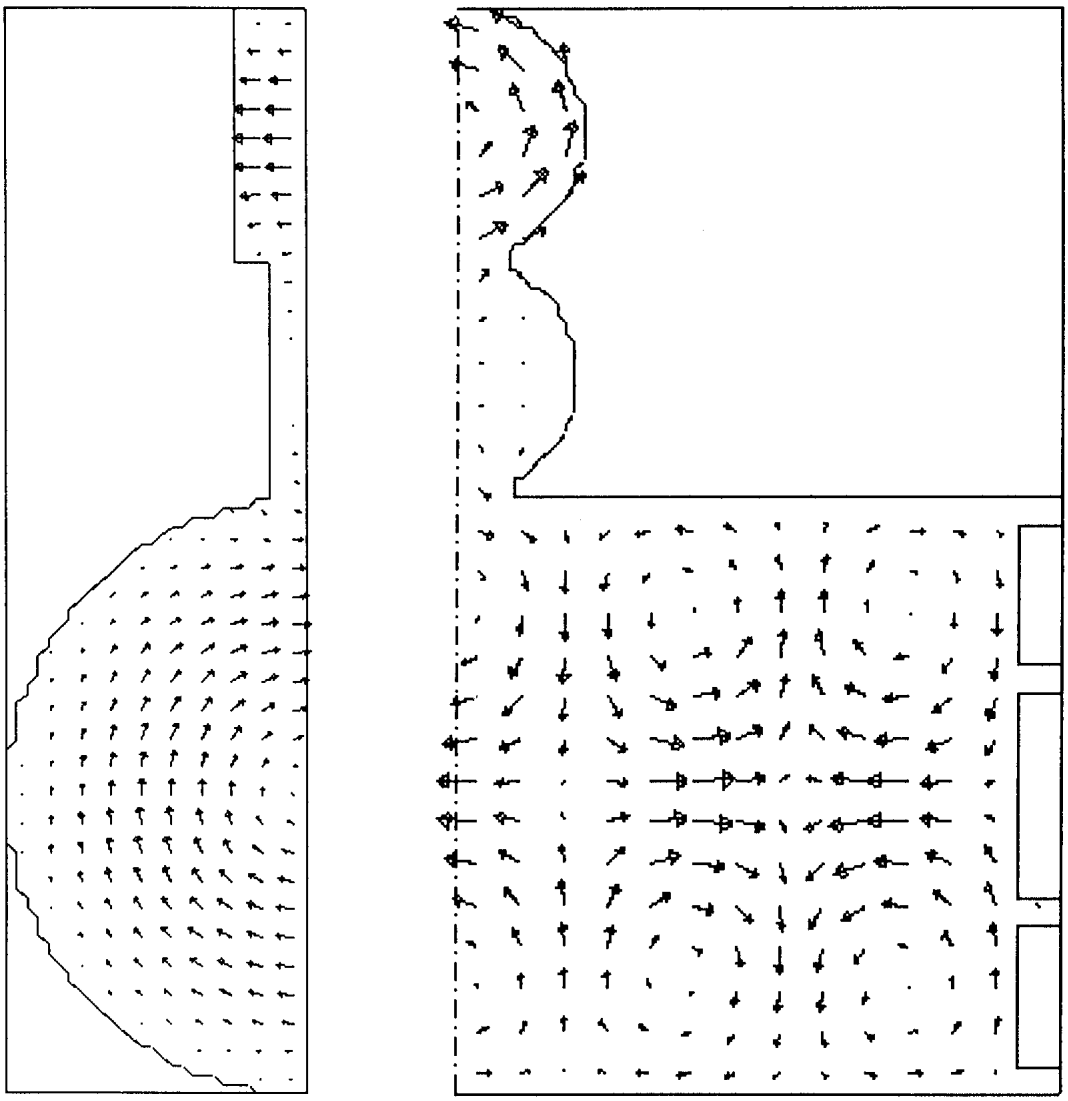

Figure 8.7: Field pattern of the $\pi/2$ mode calculated with the MAFIA code. The electric field (left) and the magnetic field (right) patterns are shown.

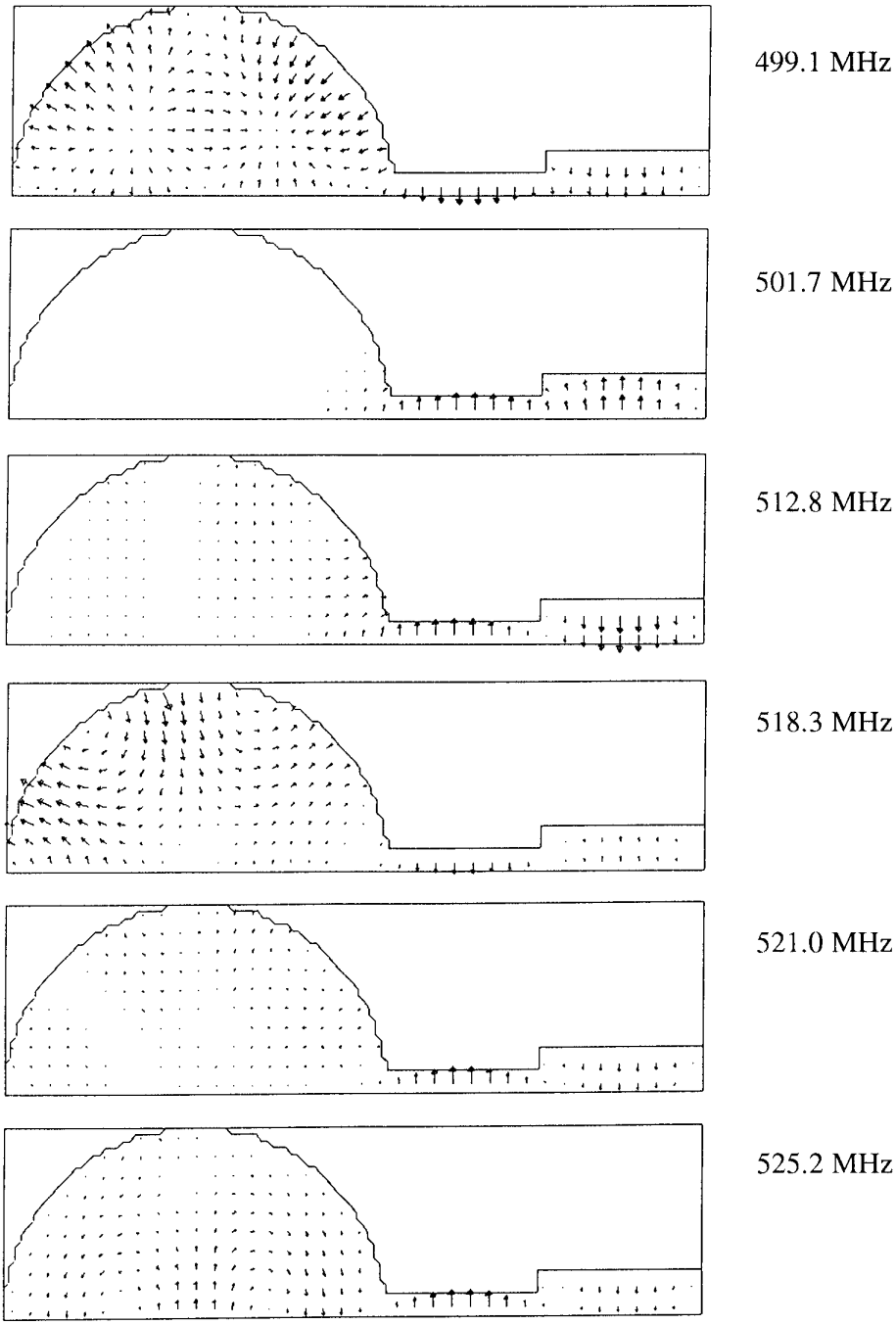

Figure 8.8: Field patterns of the parasitic modes, with frequencies close to the operating mode.

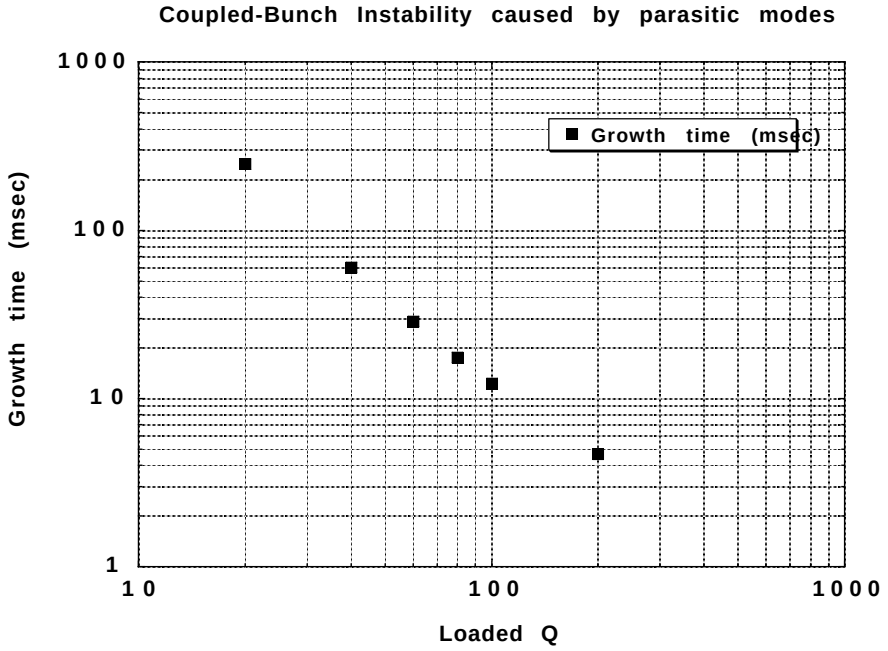

Figure 8.9: Fastest growth time of the coupled bunch instability caused by the parasitic modes plotted against the damped Q value.

reduced below 100, the instability growth time becomes longer than 10 ms, where the beam instability can be controlled by a feedback system.

Results of Cold Model Test

Two aluminum 1/5 scale cold models have been fabricated to confirm the design described above. They are equipped with two tuners for each of the accelerating, coupling and storage cavities. The resonant frequencies of the three cavities are adjusted by these tuners to coincide with each other. There is no damping structure on the coupling cavity of the first model. The measured Q value of the $\pi/2$ mode is 3.3×10^4, which corresponds to 1.40×10^5 for a full scale copper cavity. The effect of the surface finish on the Q value has been estimated by measuring the Q value of a pillbox cavity of the same material, same surface finish and same inner shape as the accelerating cavity of the cold model ("reference pillbox"). Taking this effect into account, the measured Q value of the $\pi/2$ mode is 0.85 times that calculated by MAFIA. The shift of the resonant frequency of the $\pi/2$ mode was measured by placing a small metallic

Table 8.3: Measured parameters of the 0 and π modes.

	f [MHz]	Q	R/Q [Ω]
0 mode	503.4	110	103
π mode	514.9	150	72

bead in the accelerating cavity to simulate the effect of detuning. The ratio of this frequency shift to the shift obtained by the same measurement for the reference pillbox was 0.069. This agrees well with the expected value 0.065. This means that R/Q of the accelerating mode is reduced by a factor of about 1/14, clearly showing that detuning of the ARES $\pi/2$ mode is greatly reduced.

The second cold model has two coaxial lines at the center of the end plates of the coupling cavity. The coupling cavity can be damped by connecting loads to these coaxial lines. The cavity surface around the inner conductor of a coaxial line protrudes into the cavity like a nose cone for concentrating the electric field and to stabilize the mode. The transmission between a beam port and an end plate of the storage cavity is shown in Figure 8.10: (a) the coupling cavity is not damped and (b) is damped. The measured Q, R/Q and frequency are listed in Table 8.3. Using the parameters in Table 8.3, the growth time of the longitudinal coupled bunch instability was calculated to be 17 ms for 20 ARESs in LER. We have also calculated the response of the growth

(a) (b)

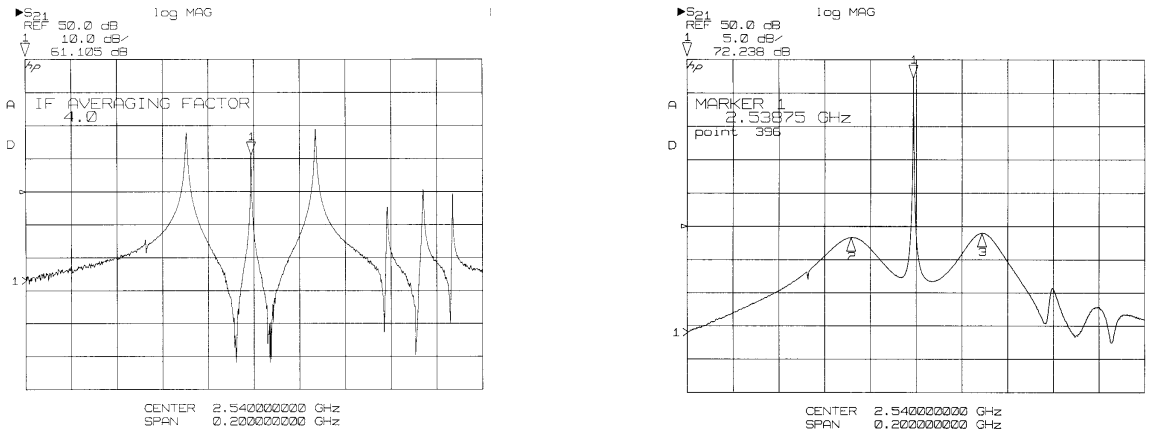

Figure 8.10: Transmission between beam ports: (a) coupling cavity is not damped and (b) is damped.

time to the skewness of the passband, which is defined as

$$\frac{|(f_\pi - f_{\frac{\pi}{2}}) - (f_{\frac{\pi}{2}} - f_0)|}{|f_\pi - f_0|}.$$

It has been found that the growth time decreases from 35 ms to 10 ms as the skewness increases from 0 to $\sim 10\%$.

Mechanical Design

The accelerating and coupling cavities are made of oxygen-free copper (OFC) to handle large power dissipation on the cavity wall. The water-cooling channels are milled out at the outer surface of the cavity. They are covered by copper plates by means of electron beam welding. Their configuration is carefully designed so that cooling water does not leak into the cavity if there should be an imperfection of brazing or welding at any connecting part. In the case of the storage cavity, the experience of the KEK APS cavities is fully utilized, since the wall loss density is not very high. Steel is used for the structural material, because it is of higher strength and is less expensive than copper. Copper is electroplated on its inner surface. The side cylinder is separated to form three parts at the nodes of the axial component of the magnetic field farthest from the center. This allows us to electroplate the structure in a moderately-sized vessel. Two end plates and three side cylinders are welded together. Welding deformation offers good electrical contact.

The accelerating and coupling cavities are joined by brazing. The coupling cavity is then bolted to the storage cavity. The two parts of ARES are transported from factory and installed at their position in the tunnel separately, where they are eventually bolted together. These procedures would be difficult if ARES is not detachable.

8.1.2 HOM-Damped Cavity

The HOM-damped accelerating cavity of the ARES is shown in Figure 8.11. The cavity has a HOM-damping coaxial waveguide which is equipped with a notch filter. Monopole and dipole HOM's excited in the cavity are coupled with the TEM and TE11 waves of the coaxial waveguide, respectively. On the other hand, the notch filter blocks the TEM wave coupled with the accelerating mode, while passing other waves of HOM's. RF waves passing through the filter are absorbed by microwave absorbers inserted from the waveguide end. This damping scheme was originally proposed independently for a crab cavity for B-factories [5] and for a damped structure for linear colliders (a radial line is used instead of the coaxial wave guide) [6]. As the absorbers, sixteen bullet-shape sintered SiC will be used.

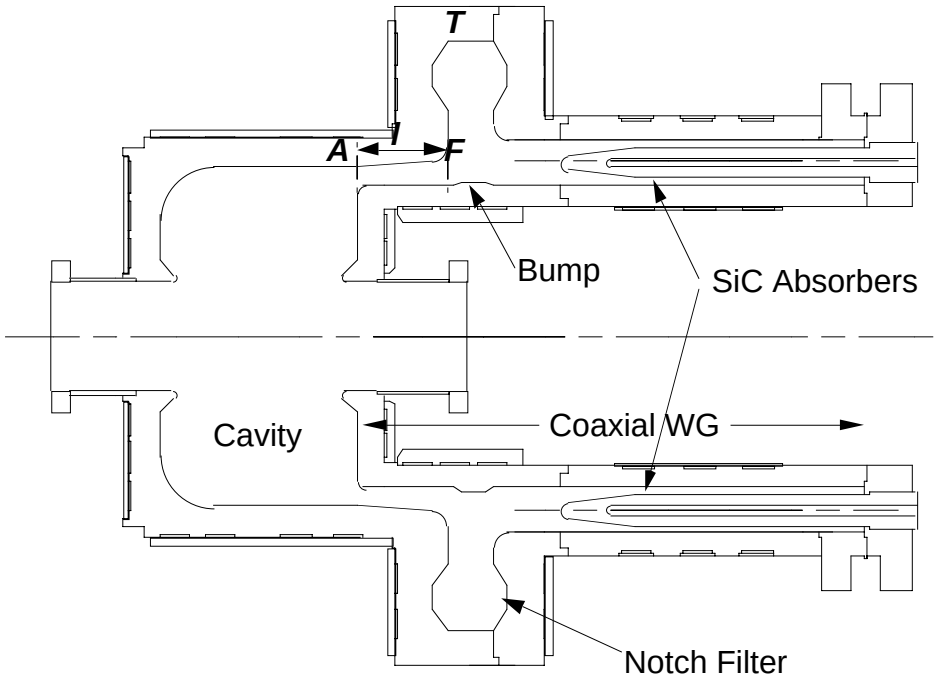

Figure 8.11: Schematic drawing of the KEKB HOM-damped cavity.

The cavity that is loaded with a coaxial waveguide is axially symmetric. This design has the following advantages:

- No concentration of wall currents of the accelerating mode assures good performance under high power operation.
- The main cavity parts can be precisely machined by using a turning lathe.
- Precise electromagnetic and thermal-structural analyses are possible by using only two-dimensional codes.

The first prototype to verify the performance in high power operation is under construction. A verification for high-current beam handling at the TRISTAN accumulation ring is scheduled in 1996.

Design

The gap dimensions of the notch filter and the coaxial waveguide have been carefully determined so as to avoid multipactoring discharges at the accelerating frequency. The S parameters of the notch filter have been calculated using the computer code HFSS (High Frequency Structure Simulator) [7]. Figure 8.12 shows the frequency responses

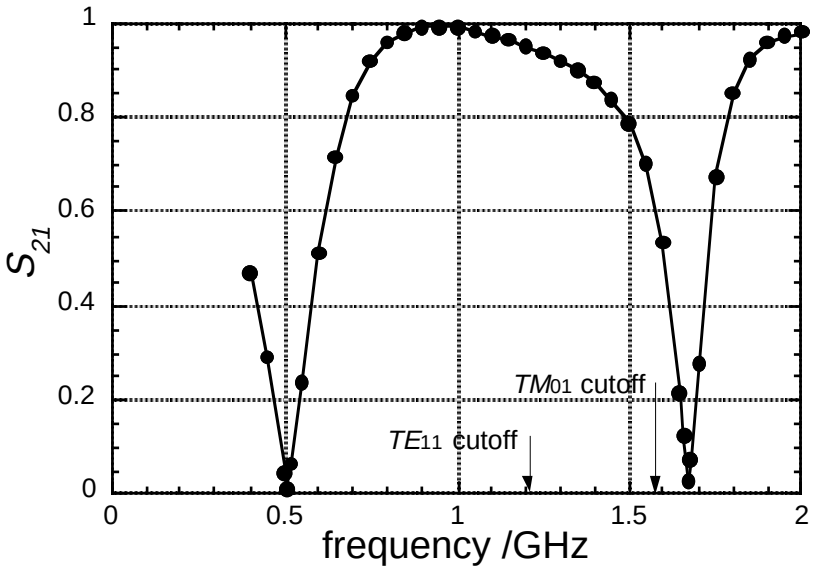

Figure 8.12: Frequency response of S_{21} of the notch filter.

of S_{21} (transmission) for TEM waves. The first stop frequency for TEM waves can be precisely tuned to the accelerating frequency 508.9 MHz by lathe-machining of the bump at the bottom of the filter structure. The TEM second stop frequency is raised to 1.67 GHz from 1.39 GHz by deforming the outer volume of the filter. The first and second stop frequencies for TE11 waves are 0.53 GHz and 1.68 GHz, respectively. Near the TEM and TE11 second stop frequencies, some HOM's may be trapped within the cavity. To avoid this problem, the beam bore diameter was increased to 145 mm. This lowers the TM01 and TE11 cutoff frequencies as indicated by the arrows in Figure 8.12.

RF Properties of the Accelerating Mode

The filter position along the waveguide affects the HOM-damping properties as well as the shunt impedance of the accelerating mode.

First, we examine the RF properties of the accelerating mode. Let us define the filter position along the waveguide by l, which is the distance between surfaces A and F, as shown in Figure 8.11. Let us also represent the stored energy and power dissipation in the cavity (the left side of surface A) by U_a and P_a, and those in the notch filter by U_f and P_f. Figure 8.13 shows the ratio P_f/P_a as a function of l, together with the response of the shunt impedance. They have been calculated using the program SUPERFISH. The notch filter functions as a quarter-wavelength resonator at the accelerating frequency. When the total electrical length from the waveguide aper-

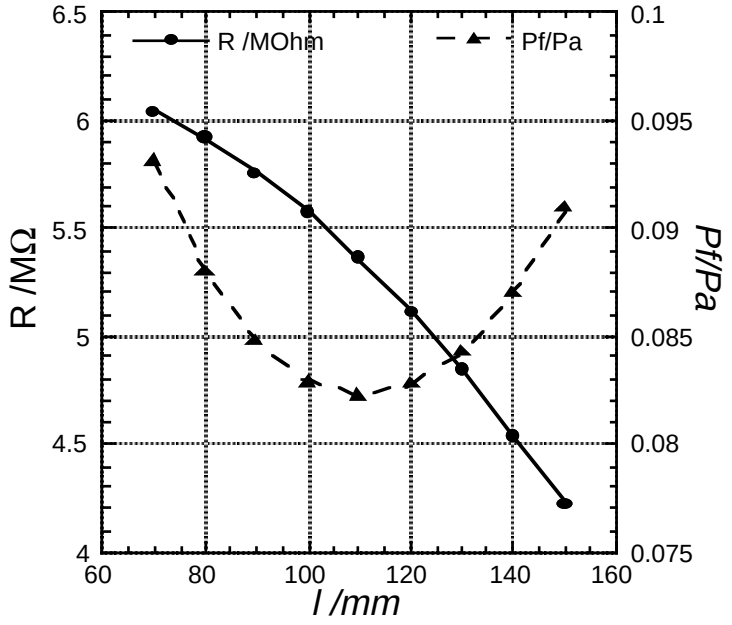

Figure 8.13: Ratio P_f/P_a and the shunt impedance are plotted as a function of l.

Table 8.4: RF parameters of the accelerating mode.

$f = 508.6\,\mathrm{MHz}$	$V_c = 0.6\,\mathrm{MV}$	$P_c = 70\,\mathrm{KW}^{(*)}$
$R/Q = 150\Omega$	$Q = 3.3 \times 10^{4(*)}$	$R = 5.0\,\mathrm{M}\Omega$

(*) a degradation of $\sim 5\%$ due to copper surface imperfections is taken into account.

ture (surface A) to the top end of the filter (surface T) is close to a half wavelength ($l = 110\,\mathrm{mm}$ in Figure 8.13), the electrically-short boundary at surface T is mapped onto surface A, and the ratio $U_f/U_a(also, P_f/P_a)$ becomes minimum. However, this is not a necessary condition in designing the choke mode cavity. For optimizing the efficiency of beam acceleration, a shorter coaxial waveguide between A and F is desirable. Figure 8.13 shows that the shunt impedance increases as l becomes smaller. The waveguide length l was determined to be 120 mm. This gives better HOM damping properties at little sacrifice of the shunt impedance of the accelerating mode. Table 8.4 is a set of cavity parameters for the case when $l = 120\,\mathrm{mm}$.

HOM Damping Properties

The distance l also changes the HOM damping properties of the choke mode cavity

Table 8.5: Ring parameters used in to calculate the growth time of the coupled bunch instability in Figure 8.14(b).

Parameters		
Beam Energy	3.5	GeV
Beam Current	2.6	A
RF Frequency	508.9	MHz
Number of Bunches	5120	
Momentum Compaction	1.5×10^{-4}	
Synchrotron Frequency	1.7	kHz
Number of Cavities	20	

(a) (b)

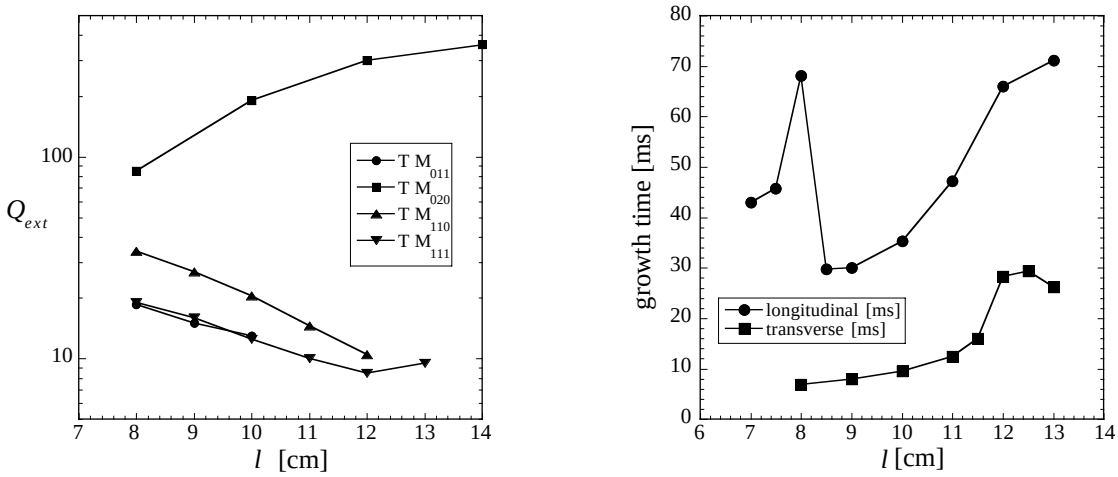

Figure 8.14: (a) Q_{ext} and (b) growth time of the coupled bunch instability as a function of the length between the cavity and notch filter l.

through Q_{ext}. Figure 8.14(a) shows the values of Q_{ext} as a function of l. The time domain method with MAFIA [8] was used in the calculation. For TM011 and TM110 modes, the time domain method was not applicable for larger l because of unwanted excitation of nearby modes in the calculation. The value of l around 12 cm provides a small Q_{ext} for the modes other than TM020. The TM020 mode needs not be damped like the TM011 mode, since R/Q of the TM020 mode is much smaller than that of the TM011 mode.

We also calculated the growth time of a coupled bunch instability as a function of l

Table 8.6: HOM impedance of the accelerating cavity of the ARES.

monopole			
f(MHz)	$R/Q(\Omega)$	Q_L	$(R/Q) \times Q_L$ (Ω)
76.2	17.4	71.5	1243
190	4.5	24.5	109
662.6	2.8	25.4	72.2
731.7	11.0	35.7	394
821.8	7.9	22.7	180
925.2	3.8	16.6	62.4
1331.9	3.2	28.7	90.7
1389.5	3.1	27.8	86.4
dipole			
f(MHz)	R/Q (Ω/m)	Q_L	$(R/Q) \times Q_L$ $(k\Omega/m)$
275.4	50.7	63.4	3.21
670.0	16.6	37.1	0.62
766.2	167	50.9	8.51
826.7	113	30.4	3.43
905.8	109	20.5	2.23
986.8	210	23.2	4.85
1067.5	68.1	10.4	0.70

by using the formulae of Sacherer [9]. The modes which are trapped in the notch filter or coaxial line have to be taken into account. The eigenmodes were calculated with the MAFIA 2D eigenmode solver. As an approximation, the absorbers were modelled by an axially symmetric structure. The permittivity was assumed to be 7, which is about half the measured value of some sample blocks of SiC [10]. This is to compensate for the packing factor of the bullet-shaped SiC. The Q value and shunt impedance have been calculated in the MAFIA postprocessor assuming that $\tan\delta$ of the absorber was 0.3. Then, the calculated frequencies, impedance and Q values were substituted in the formulae of Sacherer with the ring parameters shown in Table 8.5. The results are plotted in Figure 8.14(b). It shows that $l = 12 \sim 13\,\mathrm{cm}$ is a good choice for l. This is consistent with the time domain Q_{ext} calculation. The growth time will be then $\sim 70\,\mathrm{ms}$ for the longitudinal instability and $\sim 30\,\mathrm{ms}$ for the transverse. The R/Q and Q values with this design are summarized in Table 8.6. However, we must be careful

about this value, because the Q calculation in the MAFIA postprocessor is based on the eigenmode that assumes no loss in the absorber.

Mechanical Design

The cavity parts, whose inner surfaces must withstand the heat due to wall currents of the accelerating mode, are made of oxygen-free copper (OFC). The coaxial waveguide parts are made of stainless steel to reinforce the entire cavity structure. Vacuum furnace brazing and electron-beam welding techniques are employed to assemble the parts. For the prototype cavity at 70-kW wall dissipation, thermal and thermal-stress analyses have been carried out using the finite element analysis program ANSYS. Figure 8.15 shows the temperature contour over the model based on the thermal analysis. The boundary conditions are as follows: on the surfaces of the cooling-water channels, the temperature is fixed at 30 °C. The outside surfaces of the cavity are thermally insulated to the air.

In Figure 8.15, there are two points with the maximum temperature rise: one is at the tip of the right nosecone; the other around the corner of the waveguide aperture. A maximum temperature rise less than 30 °C is acceptable. Therefore, the prototype cavity will be capable of stable continuous operation at the design value of the wall dissipation.

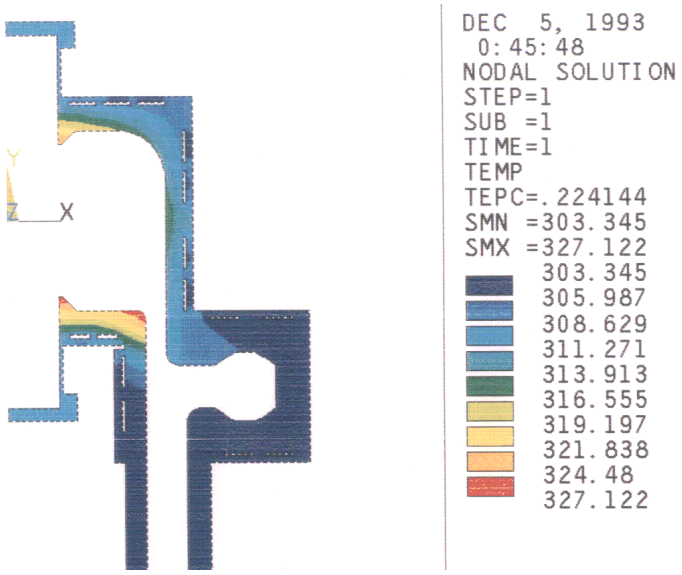

Figure 8.15: Temperature contour over the model resulting from the thermal analysis.

8.1.3 HOM Absorber

For HOM absorption, sixteen bullet-shape sintered SiC (silicon carbide) ceramics are inserted from the end of the coaxial waveguide, as shown in Figure 8.11. The absorber is 40 mm in diameter and 400 mm in total effective length, including a 100 mm nose-cone section. Each SiC absorber is directly cooled by cooling water through a water channel that is bored inside. The HOM power to be handled will be on an order of $\sim 10\,\mathrm{kW}$ per cavity, leading to ~ 1 kW per absorber. Figure 8.16 shows the frequency responses of the dielectric constant ϵ' and the loss tangent $\tan\delta$, which have been measured using a dielectric probe kit (HP85070B). The reasons for choosing SiC ceramics are as follows:

- SiC is a fine and dense ceramic material which has high mechanical strength, a low outgassing rate, and is chemically inert.
- SiC has a relatively high thermal conductivity of $\sim 120\,\mathrm{W/mK}$ at room temperature, which is about one half that of aluminum (230 W/mK).

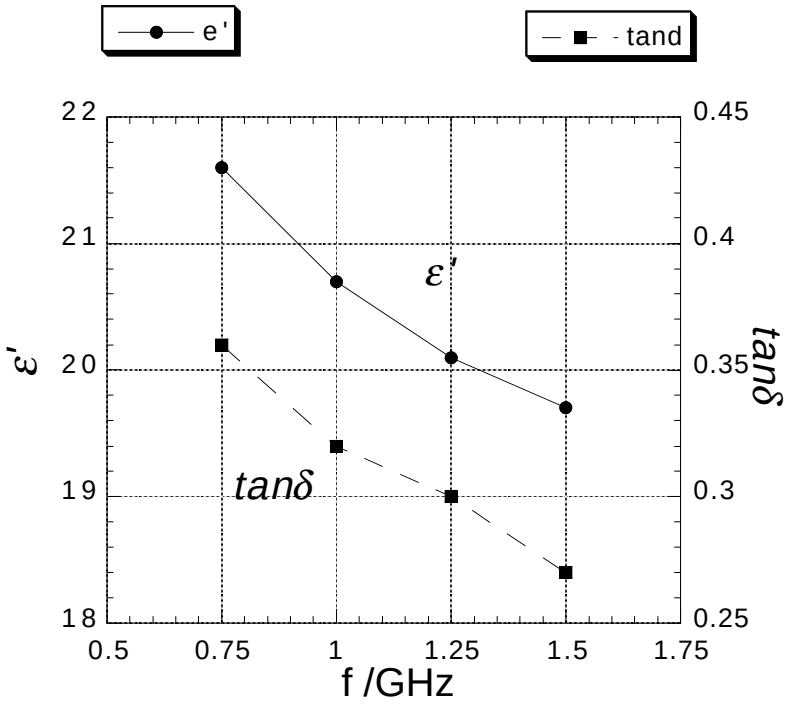

Figure 8.16: Dielectric constant and loss tangent of the SiC ceramics are plotted as a function of the frequency.

- At the 2.5-GeV electron linac of KEK, nearly two hundred SiC absorbers (diameter = 24 mm, length = 300 mm) have been used for the S-band waveguide loads without any trouble for about ten years. A prototype of the S-band SiC absorber has been tested up to a peak power of 10 MW with a pulse width of 3.5 μsec at 50Hz, corresponding to an average power of 1.75 kW [11].

Among these reasons, the third one encouraged us most to use SiC ceramics. A prototype of the SiC absorber for the KEKB cavity was fabricated to verify its performance in a vacuum environment. Figure 8.17 shows the layout of the high power test. The prototype absorber was inserted from the end of an L-band rectangular waveguide (WR650), where the standing-wave ratio VSWR was measured to be ~ 1.1. A metal O-ring was used for the vacuum seal between the SiC ceramics and the SUS flange. The vacuum pressure was about $10^{-9} \sim 10^{-8}$ Torr. The high power test was carried out using a pulsed klystron ($f = 1296$ MHz) up to a peak power of 105 kW with a pulse width 538 μsec at 50 Hz, which corresponds to a average power of $\sim$2.8 kW. The prototype SiC absorber functioned normally without any vacuum, thermal, or discharge problems. The outgass rate of the SiC ceramics was also measured using a cylindrical sample (diameter = 50 mm, height = 50 mm). After baking for 24 hours at 150°C, the outgass rate at room temperature was 3×10^{-12} Torr$\cdot l$/s$\cdot$cm^2.

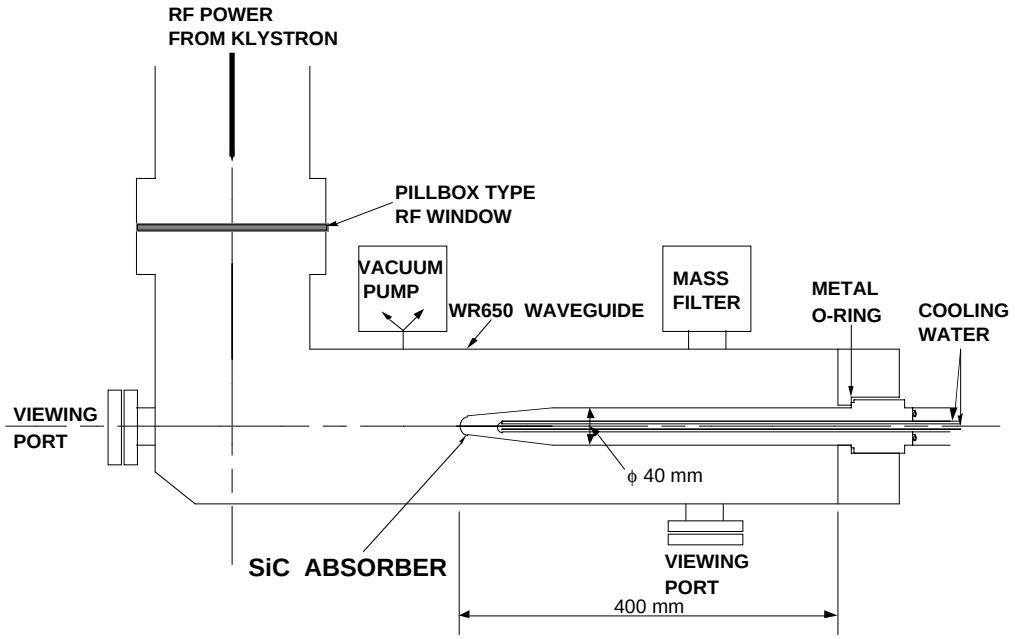

Figure 8.17: Layout of the high power test.

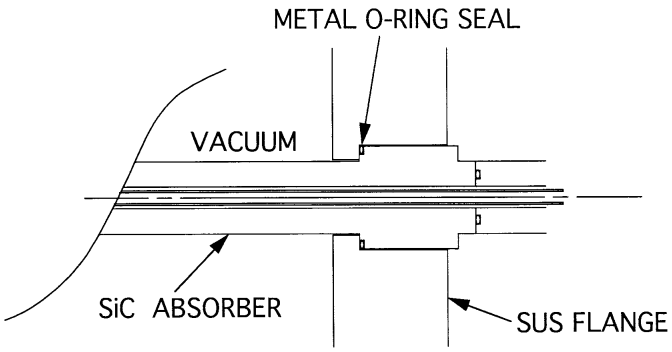

Figure 8.18: Prototype of the SiC absorber using a metal O-ring for vacuum sealing.

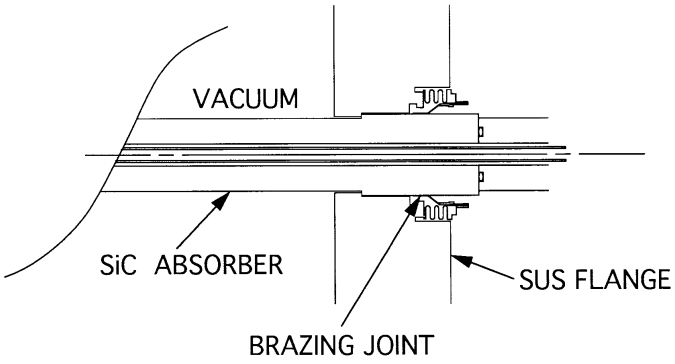

Figure 8.19: Next prototype of the SiC absorber using a brazing joint. The SiC ceramics is directly brazed to the copper sleeve.

For the second prototype cavity, we are planning to braze a thin copper sleeve to an SiC ceramic absorber for vacuum tightness. Figures 8.18 and 8.19 show an SiC absorber structure that uses a metal O-ring seal and another that uses a brazing joint, respectively. For both structures, a series of heat-cycle tests will be carried out, which simulates the baking processes, in order to study the reliability of the vacuum tightness during long term operation.

8.1.4 Input Coupler

Requirements

The most important parameters for the coupler are the transmitted RF power and its frequency. At the present stage the cavity for KEKB requires $\sim$ 400 kW (CW) RF power at 508.9 MHz. In order to maintain stable operation at $\sim$ 400 kW, the coupler is required to be able to transmit the RF power that is much larger than $\sim$ 400 kW. We have thus set the target value of the transmitted RF power to be $\sim$ 800 kW (CW) that is twice the required power.

The requirements for the mechanical structures are as follows:

1. The RF power is fed from a klystron through the WR1500 rectangular waveguide.
2. The coupler couples with the cavity by a loop (magnetic) coupling.
3. The size of the coupler port of the cavity is designed for the WX77D coaxial waveguide.
4. The ceramic window must be shielded from the beam and the cavity surface. This is to reduce direct irradiation by the x-rays and charged particles produced by collisions between the beam, field-emitted electrons, sputtered ions and residual gases and to avoid the adsorption of Cu evaporated from the cavity wall.
5. The coupler matches the APS cavity in TRISTAN, because the coupler of the APS will be used for the first beam test of the cavity.

The coupler has several transitions. Every transition is designed so that the its VSWR is less than 1.05 and that of the coupler assembled with the transitions is less than 1.1 at 509 MHz.

Design Status

The design of the input coupler is based on the structure of the output coupler of the UHF klystron for TRISTAN. The first design for the RF structure was completed by using the computer simulation code HFSS. The mechanical design is in progress. The RF properties of the coupler will be measured by a low-power model so as to confirm the simulated results. A high-power test for the coupler is planned for the summer os 1995 with an RF power up to 800 kW (CW).

Choice of Window Structure

Many problems with the coupler are related to multipactoring on the window. Several experiments and analyses of the ceramic window in couplers suggest the following [12, 13]: the uniformity of the electric field distribution around the window is very important for preventing the local heating of the ceramic induced by multipactor; the multipactor induced by an electric field that is perpendicular to the window causes the damage on the surface, while the multipactor induced by the parallel field causes no serious problem.

Two types of ceramic windows are in use for the coupler at KEK. One is a cylindrical-type ceramic window that has been used in the APS cavity. It was tested at up to 300 kW (CW) RF-power [14]. The other is a disk-type ceramic window that has been adopted for the UHF (508 MHz) klystron. It transmits 1.2 MW (CW) RF-power [12]. Since our target value for the transmitted RF-power is 1MW (CW), we chose the disk-type ceramic as the window for the coupler.

The disk-type ceramic window is contained in a coaxial waveguide. The waveguide near the window has an impedance matching section, because the permittivity of ceramic is about nine.

One of the typical matching sections is a choke-type structure. The output coupler of the klystron and the input coupler of the superconducting cavity (SCC) of the TRISTAN have the choke structure. (Recently a high-power test of the SCC coupler was successfully performed up to an RF power of 800 kW (CW) [15].)

An over- and under-cutting (OUC) is another structure for the matching section. This structure is in use for the couplers of the high-power models of the RFQ [16] linac and DTL [17, 18] for the Japanese Hadron Project (JHP). For the RFQ the coupler transmits an RF pulse that is 300 kW peak, with 300 μsec duration at 50 Hz. The transmitted RF pulse for the DTL coupler is 150 kW peak, with 600 μsec duration at 50 Hz.

Two types of couplers with choke or OUC structures will be made for the high-power test.

Design

The coupler consists of three transition sections:

1. The door-knob transition between the WX152D coaxial wave guide and the WR1500 rectangular wave guide;

2. The disk-type ceramic window in the WX152D waveguide;

3. The transformer between the coaxial wave guide of the WX77D and that of the WX152D.

The door-knob transition with a capacitive iris has a wider band width. A schematic view of the transition is shown in Figure 8.20. The calculated VSWR is shown in Figure 8.21.

The choke and OUC structures of the window are shown in Figures 8.22 and 8.23. Both figures include the transition from the WX152D coaxial waveguide to the WX77D coaxial waveguide. The waveguide has bumps for window shields. The VSWRs of the transitions with the window are plotted in Figure 8.24. Figure 8.25 shows the radial dependence of the electric field strength at a location 1 mm away from the window surface. The value of the ordinate is normalized to the field strength on the surface of the inner cylinder of the WX152D coaxial waveguide. This plot shows: (1) that the uniformity of the field strength of the OUC structure is better than that of the choke-type structure; (2) that the electric field strength of the choke-type structure is about 70% of the OUC structure near the inner triple junction of the window. Figures 8.26 and 8.27 show the electric field lines when the maximum electric field is at the center of the ceramic. These show that the direction of the electric field is almost parallel to the window for the OUC structure, while for the choke structure the lines concentrate in the tip of the choke.

The window is $5/8\lambda$ away from the detuned short plane (DSP). The DSP of the coupler is located about 55 mm inside the cavity wall.

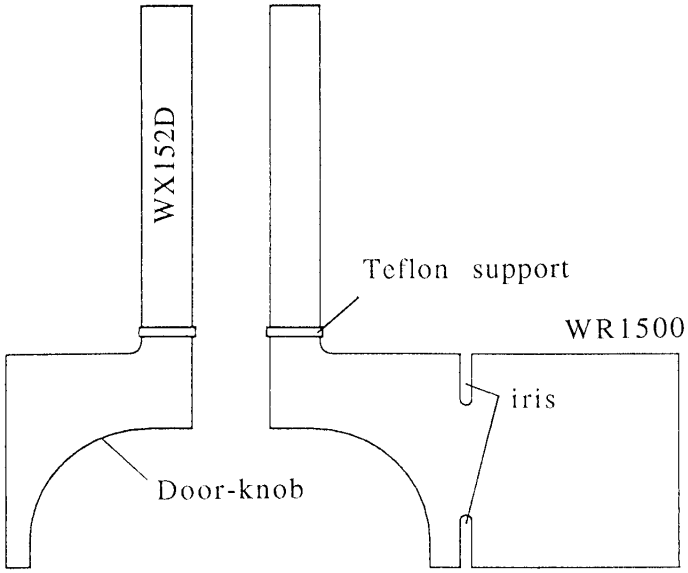

Figure 8.20: Schematic view of the door-knob transition.

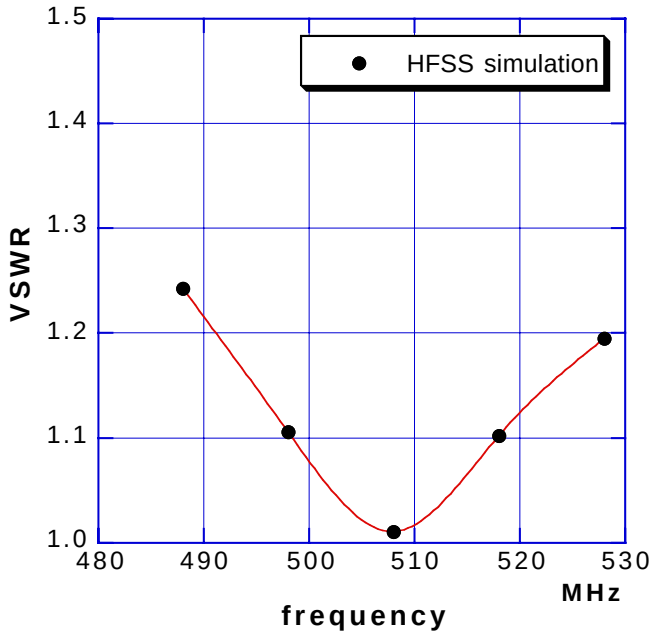

Figure 8.21: Calculated VSWR of the door-knob transition.

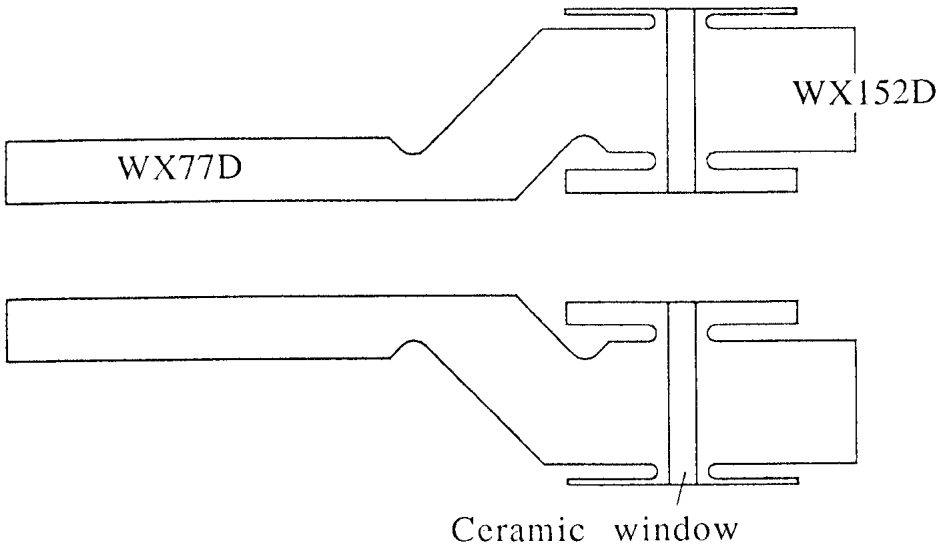

Figure 8.22: Choke structure of the ceramic window with the transition between the coaxial waveguides.

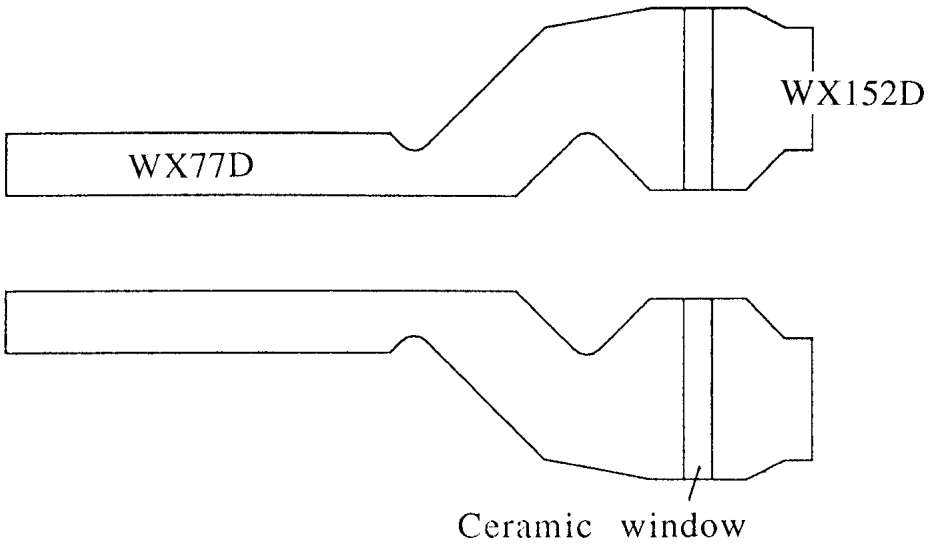

Figure 8.23: Over- and under-cut (OUC) structure of the ceramic window with the transition between the coaxial waveguides.

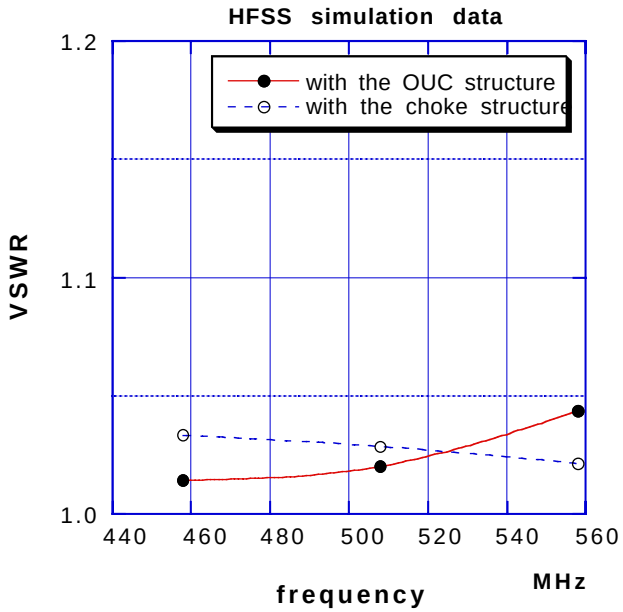

Figure 8.24: Calculated VSWR of the choke and OUC structures with the transition between the coaxial waveguides.

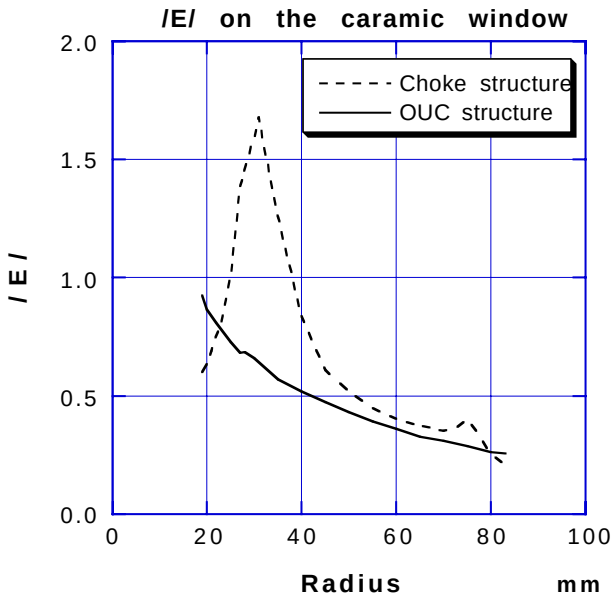

Figure 8.25: Asolute strength of the electric field. (Simulation) The abscissa is the radial direction of the window. See the text for the unit of the ordinate. The solid line is the OUC structure data and the dotted one is the data of the choke structure.

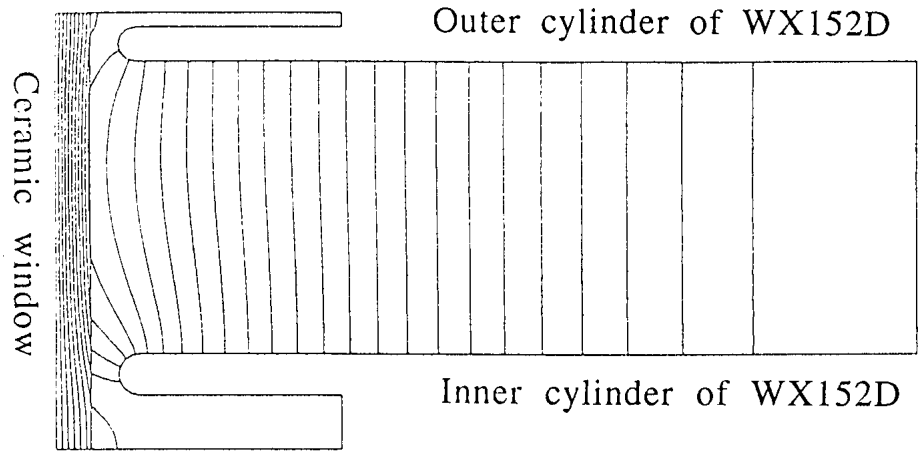

Figure 8.26: Line of the electric force for the choke structure. (Simulation)

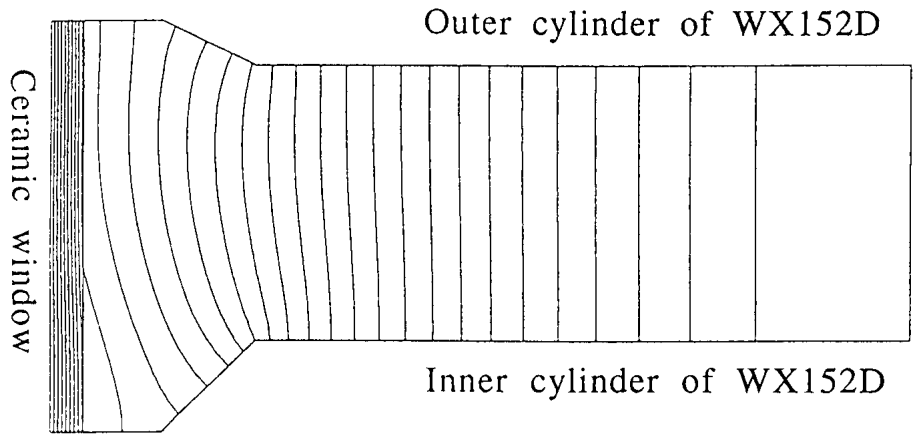

Figure 8.27: Line of the electric force for the OUC structure. (Simulation)

8.1.5 Summary

The ARES structure, where an accelerating cavity is resonantly coupled with a low-loss energy storage cavity, is expected to be a breakthrough for high-current, low-emittance beam accelerators such as KEKB. The results of 1/5-scale ARES model cavities are very encouraging. The fabrication of a full-scale storage cavity model, operating in the TE013 mode, is under way.

In parallel with the development of the ARES structure, the first prototype of the accelerating cavity, which will be employed as a part of the ARES scheme, is currently being fabricated in order to verify its performance in high power operation. The cavity has a coaxial waveguide with a notch filter to block the TEM wave of the accelerating frequency while passing other waves of HOM's to the load.

As the HOM load, sixteen bullet-shape sintered SiC absorbers will be used. SiC is a fine and dense material with high mechanical strength and relatively high thermal conductivity. It has been experimentally shown that a single SiC absorber can handle an average RF power of 2 kW, and that the outgass rate is as low as those of such metals as copper and stainless steel.

The RF window is another key issue. Two types of coaxial RF windows that can transmit CW RF power of 500 kW have been designed. Cold models of both types are currently being fabricated, and a series of high-power tests are scheduled for the summer of 1995.

8.2 Superconducting Cavity

8.2.1 Introduction

At KEK the superconducting (SC) RF system for the TRISTAN Main Ring has been successfully operated since 1988. On the basis of extensive experience in its construction and operation, the application of SC cavities to KEKB have been studied.

An advantage of the SC system is that a relatively small number of cavities can provide the required RF voltage without greatly increasing the impedance of the system for higher order modes (HOMs). This is because of the high accelerating field in the SC cavities. Due to recent technologies the field gradient of SC cavities can exceed 5 MV/m in large-scale applications. It is higher than typical normal conducting cavities by a factor of $3 \sim 5$. In addition, because of the high values of the unloaded Q, the SC cavities do not require a very high R/Q. Consequently, a HOM damping system with SC cavities will be less complicated than normal-conducting cavity systems.

Another advantage of the SC cavity system is that it is fairly immune against the coupled-bunch instability arising from the accelerating mode. As discussed in chapter 4, a consistent set of operating parameters was obtained for the HER, while the growth time is still fast in the LER. In addition, a large refrigerator that has been used for the TRISTAN SC cavities in the Nikko straight section can be re-used in KEKB. From these points, in the HER the SC cavity is considered to be a good candidate for the accelerating cavities.

8.2.2 R&D Status

A preliminary design of the cavity cell structure has been completed. An aluminum model and two niobium test cavities have been built. The HOM characteristics of the aluminum test cavity have been measured using ferrite absorbers that are attached to the beam pipe. Sufficient HOM damping has been observed. In vertical cold tests of the Nb cavities, a gap voltage of 3 MV has been achieved. A bench test of TRISTAN-style input couplers has shown that they can transmit a traveling wave RF power of 850 kW. A prototype module including these components (Figure 8.28) is currently being prepared for a beam test at the TRISTAN Accumulation Ring. The test is scheduled for 1996. The goal is to store a total current of 0.5 A.

Cavity Shape

A single-cell cavity design has been chosen, so as to reduce the number of HOMs as well as to minimize the coupler power. The concept of HOM damping is based on the

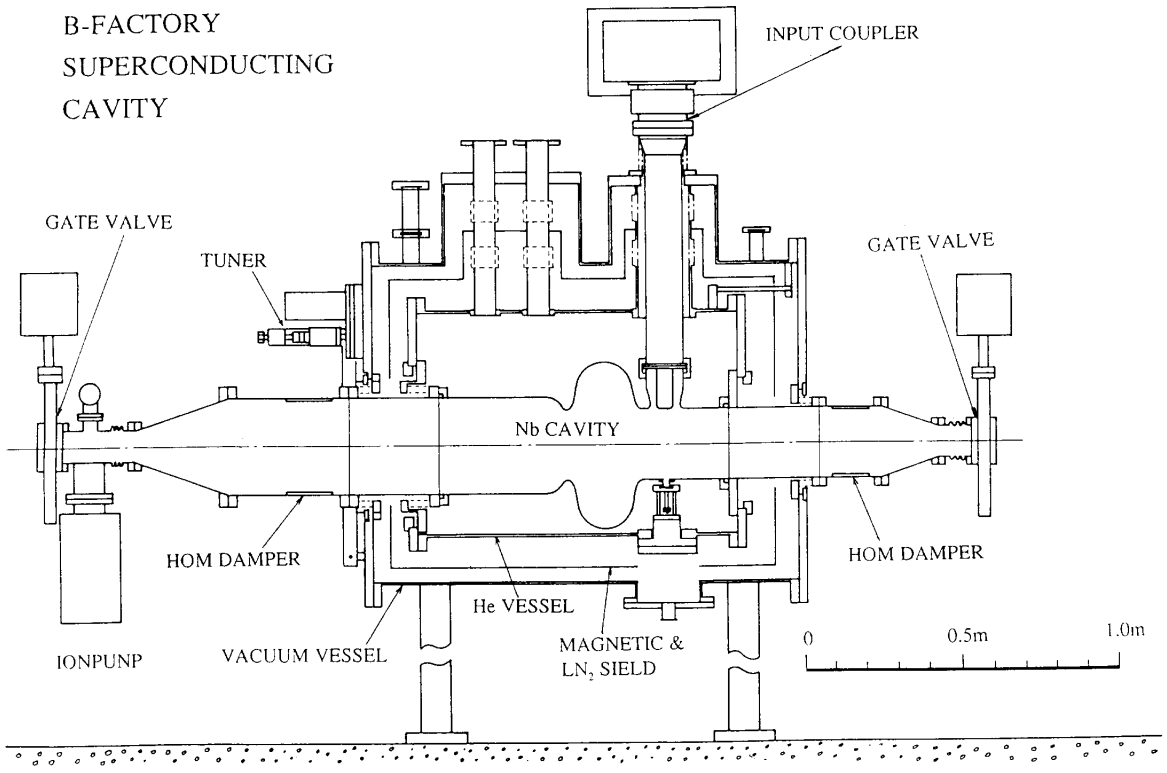

Figure 8.28: A cryomodule for a SC damped cavity for beam testing at the TRISTAN Accumulation Ring.

single-mode cavity idea, proposed by T.Weiland in 1983 [19]. All HOMs of a cavity are extracted out through large beam holes towards the beam pipes. They are damped by ferrite absorbers attached on the inner surface of the beam pipes. This scheme is favored for the SC cavities. Even if the large beam holes reduce the R/Q somewhat, the high impedance of the accelerating mode can be maintained, because of the high Q value of the SC cavities.

The spherical cell shape of the cavity with large beam holes was optimized by using computer codes, URMEL and SUPERFISH [20]. The diameter of the hole (220mm) was chosen to maintain the desired coupling of the lowest monopole modes of TM011 and TM020. Furthermore, a large cylindrical beam pipe (LBP) of 300 mm diameter is connected on one side to obtain a sufficient coupling of the lowest dipole modes, TE111 and TM110. This cylindrical geometry allows easy fabrication and surface treatment in contrast to a grooved beam pipe [21]. The external Q of each HOM was estimated using the tuning curve method by J. Slater [22]. The cavity parameters of the accelerating mode are summarized in Table 8.7. The design of the cavity shape is

Table 8.7: Cavity parameters of the accelerating mode (by SUPERFISH).

frequency	508	MHz
gap length	243	mm
dia. of iris	220	mm
dia. of LBP	300	mm
R/Q	93	Ohm/cavity
loss factor	0.074	V/pC
$E_{surfacepeak}/E_{acc}$	1.84	
$H_{surfacepeak}/E_{acc}$	40.3	Gauss/(MV/m)

R is defined by V^2/P.

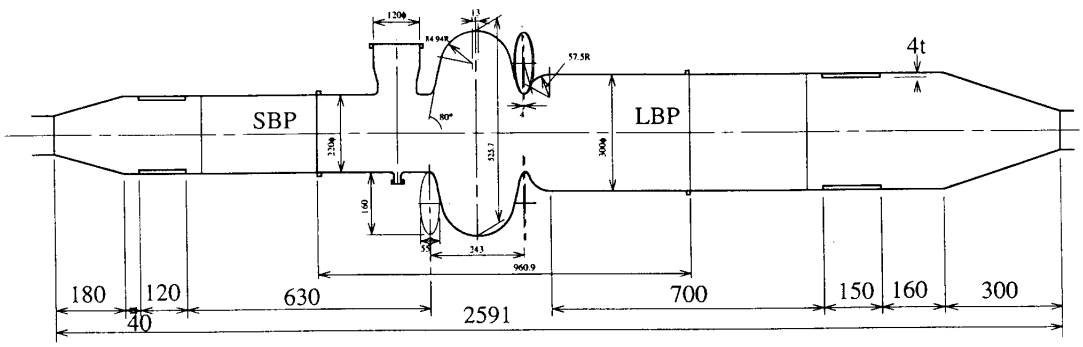

Figure 8.29: Optimized cell shape and ferrite absorbers.

shown in Figure 8.29.

HOM Damping

IB-004 ferrite has been chosen as the HOM absorber, because of its superior RF properties around 1 GHz. The damping characteristics of the absorbers strongly depend on geometrical parameters: the distance from a cell, the length and the thickness of ferrite, and the taper angle between absorbers and a beam duct. These parameters are optimized by using the computer code SEAFISH, which can calculate the Q value of monopole modes for the cavity, including the effects of resistive materials.

An aluminum model cavity was built to confirm the damping characteristics. The experimental results using full size ferrite absorbers have demonstrated the validity of

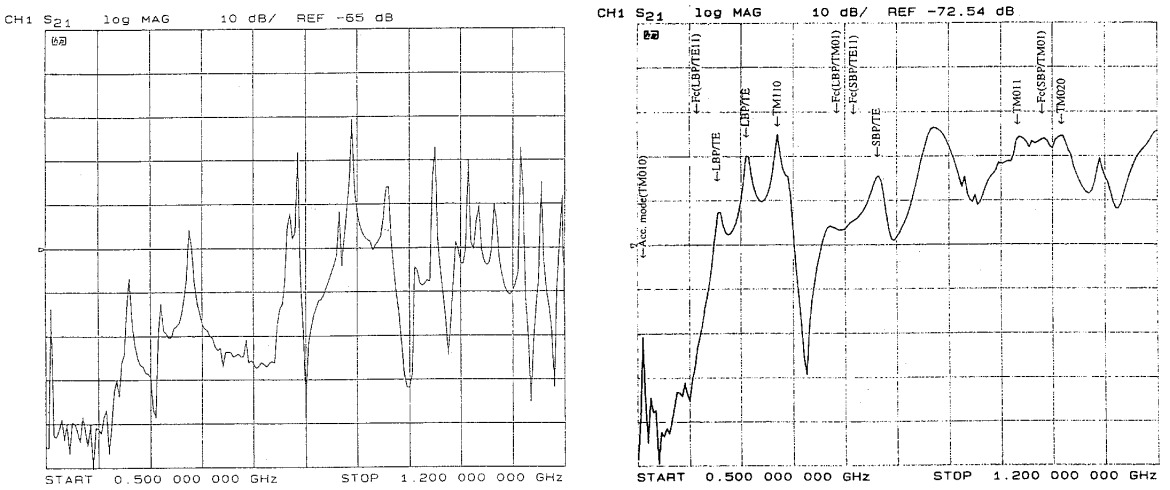

Figure 8.30: HOMs of an Al model cavity with and without ferrite absorbers. The horizontal axis shows the frequency from 0.5 to 1.2 GHz.

the calculations. It has been shown that both the monopole and dipole modes have Q values close to 100. The HOM spectra in an aluminum model cavity with and without absorbers are shown in Figure 8.30. The measured frequency and the Q value of HOMs are listed in Table 8.8 together with the power generated by a beam of 1.1A in the HER.

Because of the short bunch length (4 mm) specified in the design of KEKB, the HOM impedance for frequencies up to 20GHz should be considered. A study using the ABCI code shows that the loss factor of the cell alone is relatively low, 0.3 V/pC. However, the total loss factor for the system has been calculated to be 2.3 V/pC per cavity. This is caused mainly by the pair of tapers that connect the cavity to beam ducts whose diameter is 100 mm. In the case of a duct with 150 mm, the loss factor is reduced to 1.5 V/pC as shown in Figure 8.31.

In this case powers of 3.5 kW and 20 kW will be absorbed by a pair of ferrite absorbers in the HER and the LER, respectively. An optimization study of the taper shape, which reduces the absorber load, is in progress.

Cavity Performance

Two Nb cavities have been fabricated and tested at 4.2 K̇ in a vertical cryostat. These cavities have identical cell shapes. One of them will be dedicated to studies of the mechanical strength of the cavity after a series of cold tests.

The cavities are made of pure Nb sheet of 2.5mm thickness. After welding was completed, the cavities were treated in the same procedure as that for TRISTAN SC

Table 8.8: Measured frequency and the Q value of HOMs together with the power generated by a beam of 1.1A in the HER.

monopole

frequency	mode	R/Q	Q	power
(measured)		(URMEL)	(measured)	
MHz		Ohm		$Watts$
783	LBP-TM01	0.12	132	-
834	LBP-TM01	0.34	72	-
1018	TM011	6.6	106	900
1027	TM020	6.4	95	201
1065	SBP-TM01	1.6	76	4
1076	LBP-TM01	3.2	65	6
1134	LBP-TM01	1.7	54	1

dipole

frequency	mode	R/Q'	Q
(measured)		(URMEL)	(measured)
MHz		Ohm/m	
609	LBP-TE11	1.9	92
648	LBP-TE11	40.19	120
688	LBP-TE11	170.4	145
705	TM110	227.3	94
825	SBP-TE11	6.16	60
888	SBP-TE11	3.52	97

$R/Q' = (R/Q)_r/kr^2, \quad (\ r = 5cm\ )$

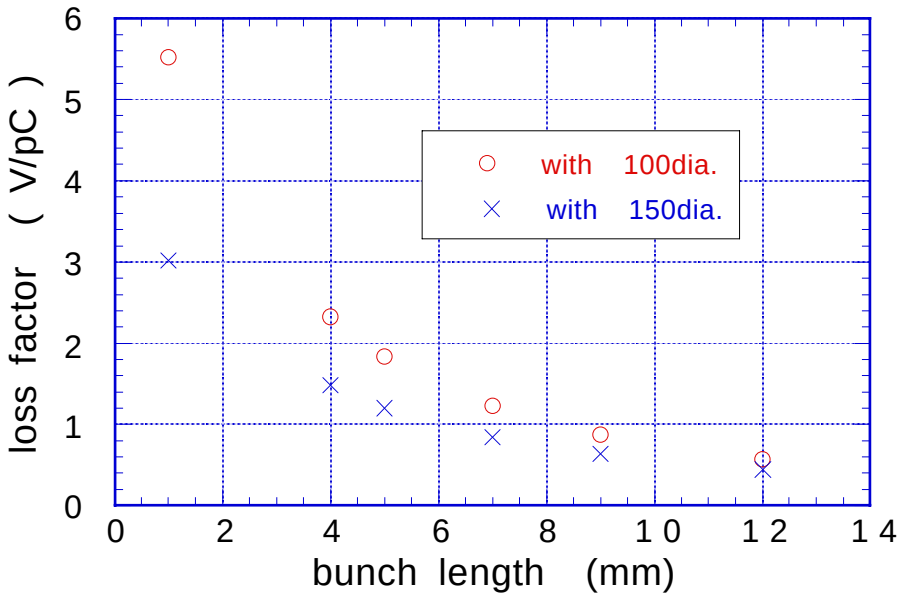

Figure 8.31: Loss factor of a cavity with a beam duct of 100mm/150mm in diameter (calculated by ABCI).

cavities: electropolishing (EP) of 90μm, annealing (700°C) and the final EP of 15μm followed by thorough rinsing with pure and ultra pure water. The results of cold tests are shown in Figure 8.32. A similar performance of Q and the accelerating field ($E_{\rm acc}$) could be obtained for both cavities, where maximum $E_{\rm acc}$ of 12.4 MV/m and 14.4 MV/m were obtained.

The field gradient is limited by electron emission, which is observed by a temperature and X-ray mapping system based on carbon resistors and PIN diodes (Figure 8.33). It has been observed that electron emission is increased for gradients exceeding 7 MV/m, if the cavity surface is exposed to air. To reduce the electron emission and to improve the stability of the RF-processed surface, ozonized ultra pure water rinsing is under study [23].

HOM Absorber

The priority of our efforts concerning ferrite absorbers has been to establish the fabrication procedure. Three bonding methods have been investigated to fix IB-004 ferrite onto the surfaces of copper beam pipes: ultrasonic soldering, vacuum brazing and HIP (Hot Isostatic Press) method. Among these methods, HIP has proven to be the most promising. There, the powder of IB-004 is packed in an iron vessel together with a

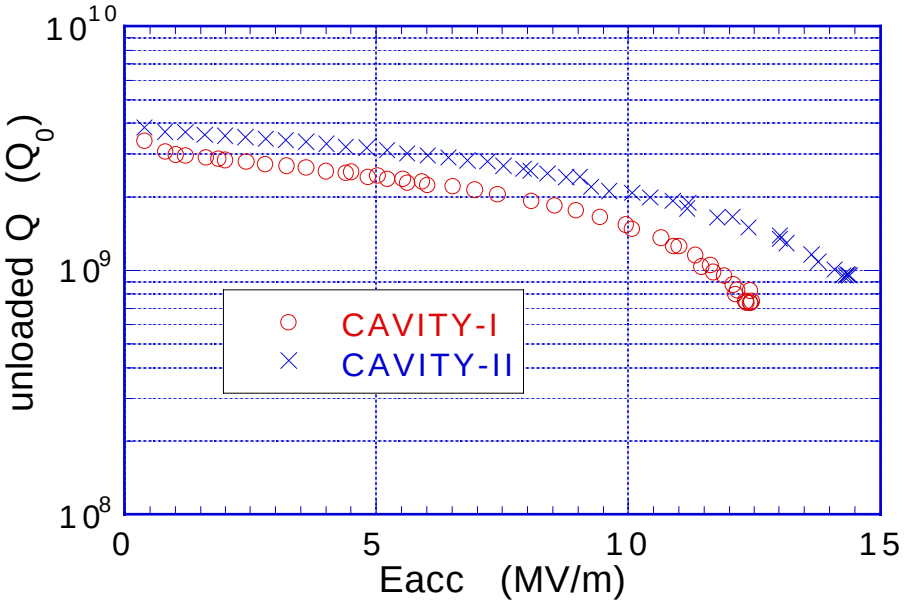

Figure 8.32: Q vs E_{acc} at vertical cold tests of the superconducting Nb cavities.

copper cylinder. After pumping the vessel to a vacuum, it is heated to 900°C in a furnace under a pressure of 1000 bar. In this vacuum environment the ferrite is sintered in a cylindrical form which is firmly attached to the inner surface of the copper [24].

To study its RF power capacity, small scale models of a HIP'ed ferrite cylinder have been fabricated. They are 15 cm long and 10 cm in diameter. A traveling RF power of 5 kW at 2.45 GHz has been applied. An RF absorption of 3.4 kW, which corresponds to 25 W/cm^2 at the front edge, caused the temperature to rise to 200°C. No cracking has occurred. The effective area of the power absorption was determined by the temperature distribution, and the average power density on the ferrite was calculated to be 14W/cm^2. An RF power test of full size models is currently being prepared.

Figure 8.34 shows a ferrite absorber for the LBP side. The out-gas rate of a full size model has been measured to be 2×10^{-7} Torrl/sec at room temperature, after baking at $150 \sim 250$°C. Pre-baking of the ferrite powder is under examination to reduce the outgas rate. The measurement of a loss factor of a ferrite wall has been conducted using the synthetic pulse method. Analytic calculations and preliminary experiments using full size models predict the loss factor of 0.3 V/pC per absorber for a bunch length of 4 mm. It will cause an additional loss of 1.4 kW for the HER and 8 kW for the LER.

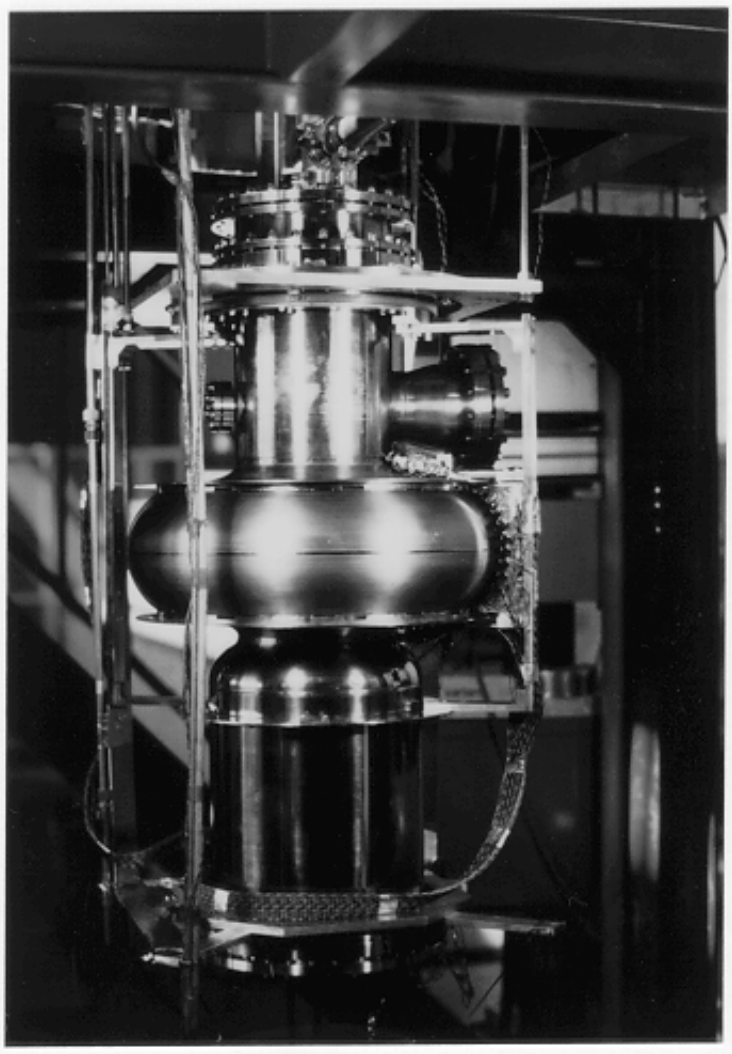

Figure 8.33: A niobium cavity module with a mapping system using 25 carbon resisters and 19 PIN photo diodes.

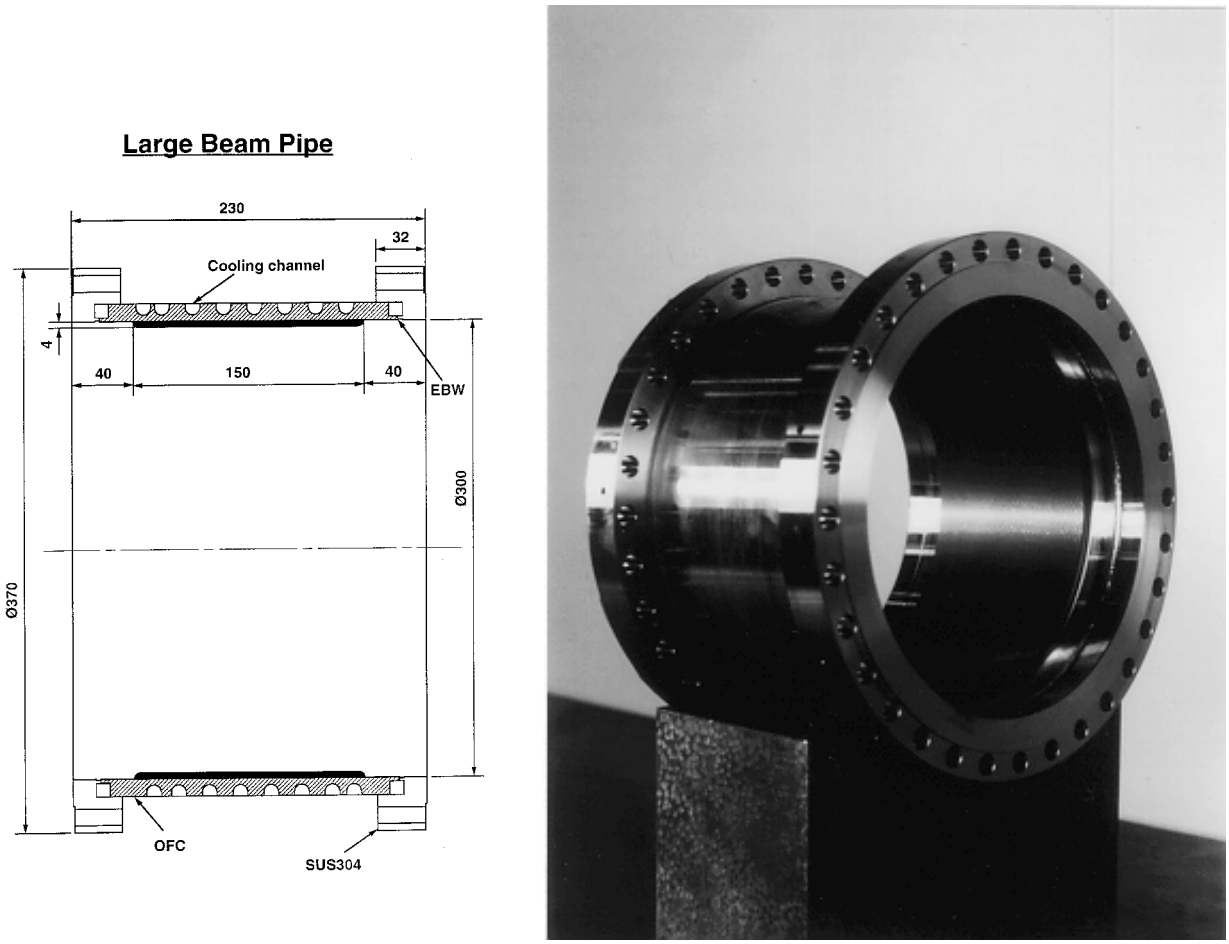

Figure 8.34: A Full size model of the ferrite absorber. The powder of IB-004 ferrite was sintered and bonded to a Cu pipe by HIPping.

Input Coupler

A coaxial antenna coupler will be used as an input coupler, which is the same type as what has been used for the TRISTAN SC cavities. A schematic drawing is shown in Figure 8.35. The ceramic window of the coupler is a 152D coaxial. The same ceramic window has been used as the output window of 1 MW klystrons for TRISTAN.

After 9 hours of RF processing, a CW-traveling RF power of 800 kW could be successfully supplied to two pairs of couplers in a test bench for more than 30 min (Figure 8.36). Most of the processing time was spent to overcome the multipactoring levels of 50 kW and 160 kW. Less processing was needed at higher power levels. A peak power of 850 kW, that was limited by the Klystron output power, could be supplied to a pair of couplers for 5 minutes, and no cracking occurred on the ceramics. A power

test with reflecting RF will be made after completing these traveling wave tests.

An analysis of cooling or heating has just started. The heating of the inner copper conductor is estimated to be 360 W for an RF power of 500 kW. The temperature rise is kept to within 10 degrees by cooling water. On the other hand, the loss of the outer conductor, which is made of copper plated stainless steel, is 160 W/m on the room temperature side and 30 W/m on the 4.2K side. This power will introduce a heat loss of about 50 W to liquid He. Optimization of He gas cooling for the outer conductor has to be done.

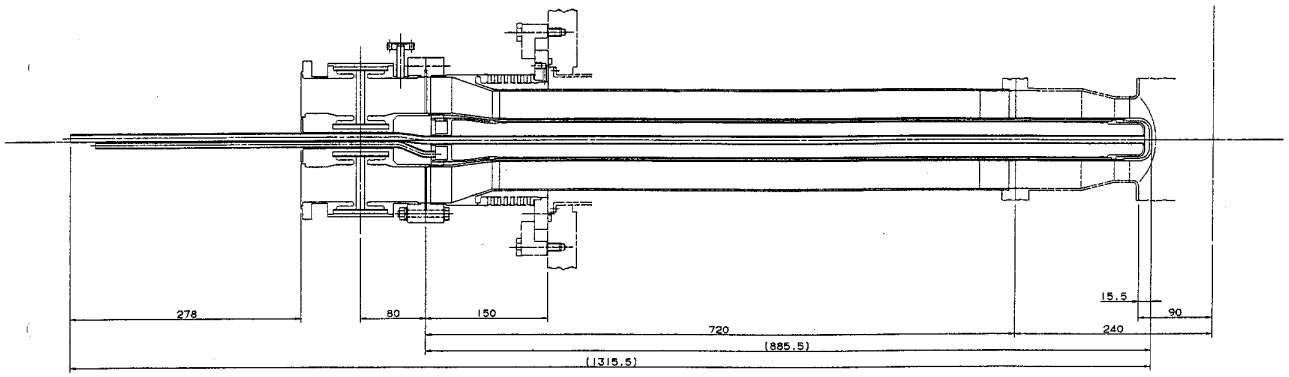

Figure 8.35: Coaxial input coupler for SC cavities.

8.2.3 Summary

The development of main components for an SC damped cavity for KEKB is in progress. A spherical single-cell cavity with large beam pipes has demonstrated satisfactory damping of HOMs using IB-004 ferrite absorbers fixed onto the beam pipes. The gap voltage of 3 MV has been obtained with Nb cavities in vertical cold tests. Tests of reduced model absorbers have been successfully conducted with RF powers of 25 W/cm^2 in peak and 14 W/cm^2 in average. No cracking of the absorbers has been observed. Coaxial input couplers that are the same as those for the TRISTAN cavities could transfer the traveling wave of 850 kW at a test bed.

The RF parameters of the HER can be realized with the recent superconducting RF technology, where $10 \sim 12$ single cell cavities will be used to maintain a beam of 1.1 A. The field gradient of each cavity is $4 \sim 6.5$ MV/m, and $400 \sim 500$ kW couplers with the $Q_{\rm ext}$ of 5×10^4 will be required. Induced HOMs of 6 kW should be absorbed by a

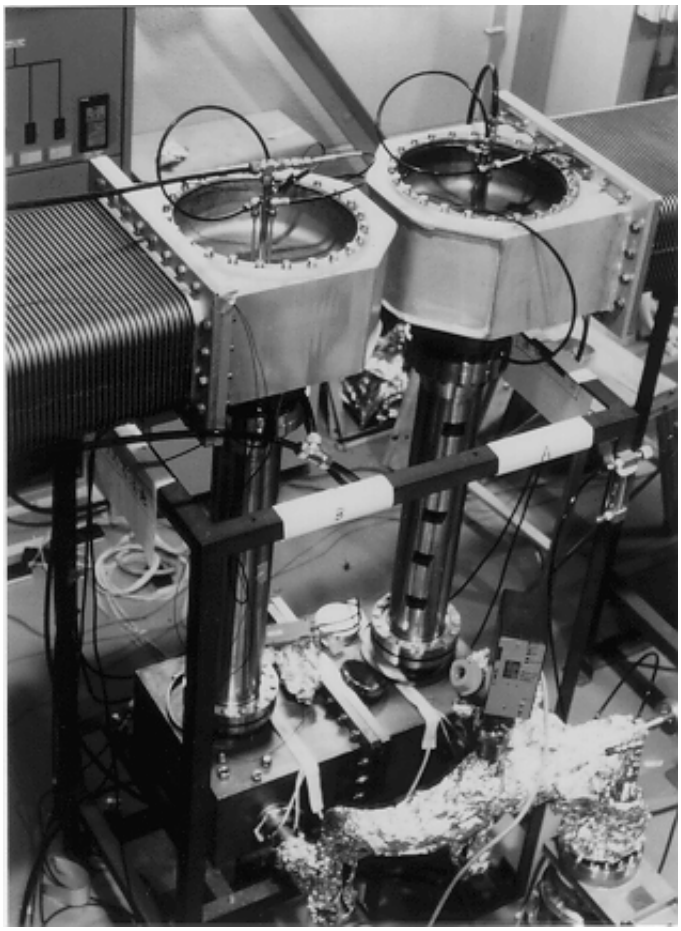

Figure 8.36: High power test bed for input couplers; a travelling RF power of 850kW was supplied to a pair of couplers.

pair of ferrite absorbers. This corresponds to an absorber power density of 3 W/cm^2. The main components, such as Nb cavities, HOM absorbers and input couplers, have been extensively tested. The experimental results demonstrate the feasibility of SC cavities for the HER. On the other hand, the application to the LER will involve many difficulties caused by the heavy beam loading under a low RF voltage. High power couplers with a low external Q and the absorption of a HOM power of 34 kW will be required.

A prototype module which includes these components and a frequency tuner is under construction for a beam test of 0.5 A in the TRISTAN Accumulation Ring. The test is scheduled for 1996.

8.3 Low Level RF Issues

8.3.1 Phase and Tuner Control

The low level RF system consists of RF signal generators, a reference line system which distributes the RF signal to all RF stations, and a low level RF control system for each RF unit. The low level system for each RF unit has feedback loops to control the cavity field, the klystron output and the cavity tuners. Phase detection is conducted at an intermediate frequency of 1 MHz.

The cavity phase should be controlled with an accuracy of less than 1 degree. This requirement is considerably tighter than that at ordinary storage rings due to the following reasons. In a double ring collider with a small β^* at the colliding point, a phase error of one ring relative to the other gives rise to a displacement of the colliding point from the minimum β^*. This results in a luminosity reduction. Another reason is that a phase error in one cavity causes extra input power and reflection power to that cavity due to the heavy beam loading. For example, if the phase of one superconducting cavity is different from the others by 1 degree, an extra power of 30$\sim$40 kW is fed to that cavity in order to keep the cavity voltage constant.

We will improve the accuracy of the existing RF reference system and phase control modules that have been used for TRISTAN. In addition, we will use a computer-aided real-time phase correction scheme, where the input power, reflection power, and cavity voltage of every cavity are monitored, and the phase error of each cavity is then calculated and corrected. This correction scheme takes advantage of the high beam-induced voltage.

In order to reduce fast ripples of the klystron power supply and phase changes of the klystron, which is on the order of ten degrees, we need a control loop for the klystron output which acts as an inner loop within the cavity voltage loop.

As seen in Figure 8.2, the ARES requires two tuner control loops: one is for the accelerating cavity; the other for the storage cavity. The accelerating cavity tuner is controlled according to its phase with respect to the input phase, which is the usual method used to compensate for the reactive component of beam loading. The storage cavity tuner is controlled not by its own phase, but by the phase of the coupling cavity; otherwise, the phase tolerance would be extremely severe.

8.3.2 Bunch gap transient

Ion-trapping is one of the problems which arises from a high electron beam current. In storage rings, some part of residual gas molecules is ionized due to collisions with

stored beams. The ions can be trapped around the beam orbit by the potential well of the electron beam. The trapped ions can: (1) shorten the beam lifetime due to the collisions, (2) give rise to a two-beam instability, and (3) affect the betatron tune.

In order to cure the ion trapping problem, several methods have been proposed. Among them, introducing a bunch gap is the most attractive solution for KEKB. In this scheme, beams are partially filled in the ring with one or more gaps, instead of being filled uniformly. The ions escape from the beam orbit to the duct wall when they encounter the bunch gap. Other methods are less attractive. For example, a method using clearing electrodes increases the ring impedance, or gives rise to local heat problems. Thus, a 5$\sim$10% bunch gap will be introduced in HER.

The bunch gap, however, modulates the accelerating field and the synchronous phase of each bunch, resulting in unequally-spaced bunches. A bunch phase modulation of $\pm$ 2.4 degrees corresponds to a longitudinal displacement of $\pm$ 1 σ_z (=4 mm) in KEKB. Furthermore, since a finite crossing angle of 2 $\times$11 mrad will be adopted, this modulation gives rise to a transverse displacement of 77 μm at the collision point, which is close to 1/3 of σ_x^*. Both effects reduce the luminosity.

The bunch phase modulation has been calculated for the cases of the ARES and SCC [25]. The results are summarized in Table 8.9. Because of the large stored energy, the phase modulation is much smaller than that of conventional normal-conducting damped cavities, which would give a modulation of typically 20$\sim$30 degrees at KEKB. The displacement of the collision point can be further reduced by introducing a corresponding gap in the positron ring (LER), which makes a similar gap transient response in LER to that in HER. Figure 8.37 shows the relative bunch phase with and without the compensation gap. By controlling the bunch charge at the compensation gap in a range from 50 to 60% of that of other bunches, the bunch phase modulation is kept below 0.5 degrees (=$0.2\sigma_z$), which is acceptable.

Table 8.9: Bunch phase modulation due to a bunch gap.

Cavity in HER	Gap length (%)	Bunch phase modulation (degree)	
		with compensation gap?	
		No	Yes
ARES	10	2.7	~ 0.3
	5	1.3	~ 0.1
SCC	10	4.9	~ 0.5
	5	2.4	~ 0.3

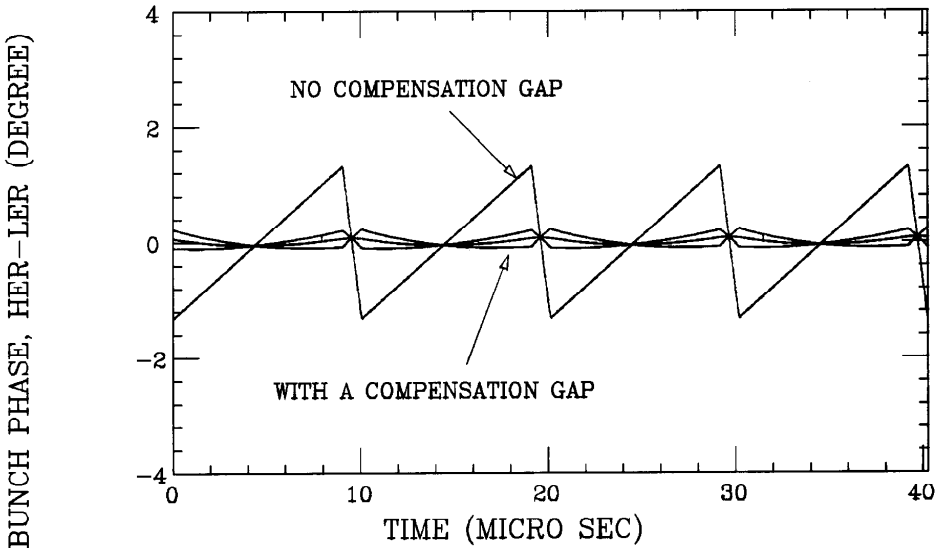

Figure 8.37: Bunch phase modulation due to a bunch gap and the effect of a compensation gap. The ARES cavities were assumed. The relative gap length is set to be 10%. The bunch current in the compensation gap is set 50, 55, and 60% of that of other bunches.

8.3.3 RF Cavity Feedback

Background

By using the ARES or the SCC the two particular beam-loading effects can be reduced: namely, the excitation of longitudinal coupled-bunch instabilities by the detuned accelerating mode, and the presence of bunch-phase modulation due to gaps in the bunch-train. Along with the development of those cavities, we are developing an RF cavity feedback system. The purpose of the feedback development is to reduce the beam-loading effects to the extent that the HOM-damped accelerating cavity of the ARES itself, without the energy storage cavity, can be used as the KEKB accelerating structure. It is obvious that, in the case where the ARES or the SCC are employed, the feedback can be used as an auxiliary means to reduce the beam-loading effects.

Here, we discuss the RF cavity feedback to be used for damping the instabilities that will arise, if the beam is accelerated solely by the HOM-damped accelerating cavities of the ARES. Figure 8.38 shows the calculated growth rates of the longitudinal coupled-bunch instabilities due to the accelerating mode of the cavities in the LER (Figure 8.38-a) and in the HER (Figure 8.38-b). The parameters used in the calculations are listed in Table 8.10. For simplicity, we refer to the mode $m = M - n$ as the mode $m = -n$. Here, M is the number of bunches, and m ranges from 0 to $M - 1$. The expected damping rate by the longitudinal bunch-by-bunch feedback system is also shown in the figure, together with the longitudinal radiation damping rate. As shown in Figure 8.38, the growth rates in the LER are higher than those in the HER, mainly due to its higher

Table 8.10: Parameters used in the instability calculations

		LER	HER	
Type of cavity		accelerating cavity of ARES		
Total cavity voltage	V_c	8.6	15.7	MV
Number of cells	N_c	20	32	
Cavity voltage/cell	V_c/cell	0.43	0.49	MV/cell
Shunt impedance/cell	R_s	5.3		MΩ
Unloaded Q	Q_0	35000		
R/Q		147		Ω
Maximum frequency detuning	Δf	−232	−82	kHz
Synchrotron frequency	f_s	1.7	1.6	kHz
Energy loss/turn	U_0	0.87	4.8	MV

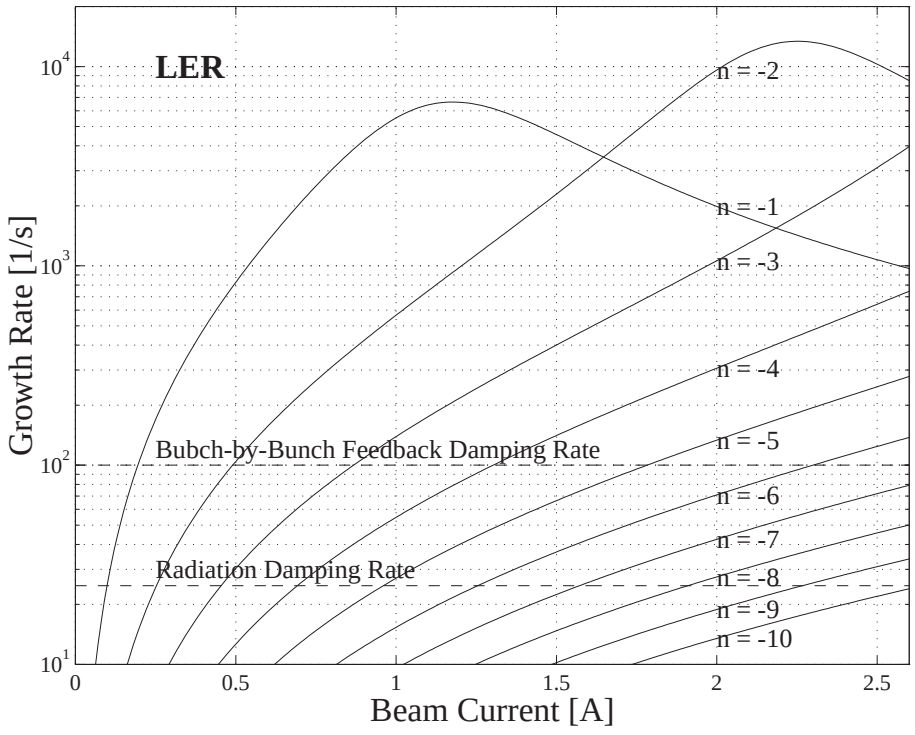

(a)

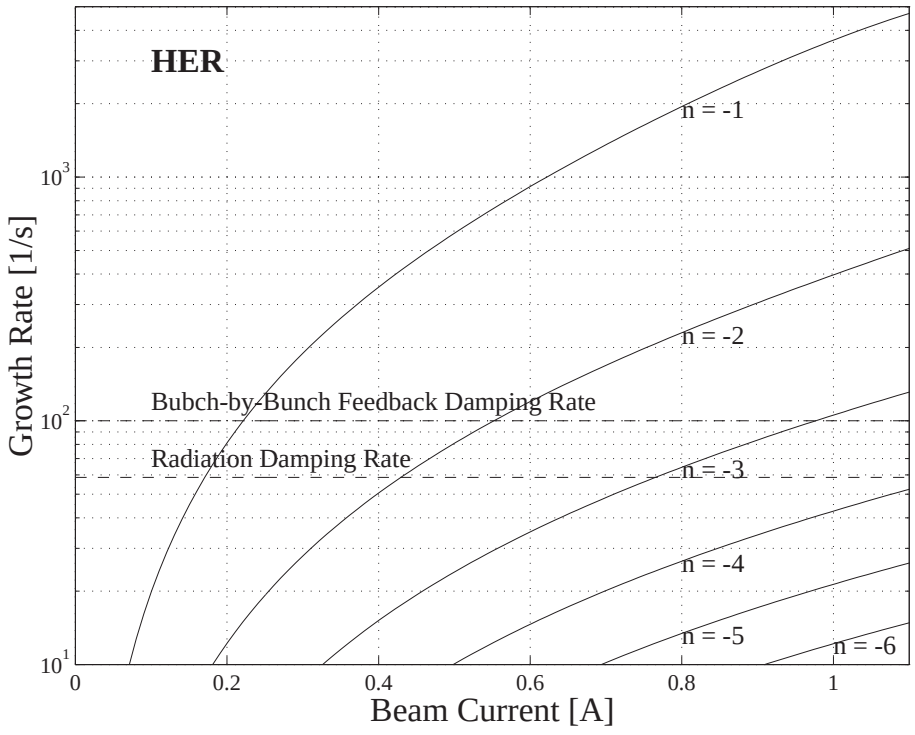

(b)

Figure 8.38: Calculated growth rates of longitudinal coupled-bunch instabilities caused by the accelerating mode of the cavities in the LER(a) and in the HER (b). The type of cavity used in the calculations is the accelerating cavity of the ARES, that is, the HOM-damped normal conducting cavity not equipped with the storage cavity.

beam current. The RF cavity feedback must reduce the growth rates, at least, down to a level which can be damped by the bunch-by-bunch feedback system. This means that the damping rate by the cavity feedback must be higher than 35 dB in the LER and higher than 23 dB in the HER. The number of modes to be damped are six ($m = -1$ to -6) in the LER and three ($m = -1$ to -3) in the HER. Since the revolution frequency of the bunches is about 100 kHz, the frequency range to be covered by the cavity feedback is more than 600 kHz in the LER and more than 300 kHz in the HER.

Principle of the System

In an RF cavity feedback, a part of the cavity voltage is picked up, filtered and vectorially added to the RF drive with an appropriate amplitude and phase so as to reduce the beam-induced cavity voltage. In this way, the magnitude of the effective cavity impedance seen by the beam is reduced. In the case of KEKB, however, an unavoidable large group delay in the feedback loop limits the bandwidth of the system to less than 100 kHz. Cables and waveguides cause a constant group delay of about 1 μs, while the klystron causes a frequency-dependent group delay of about 0.6 μs at maximum. To circumvent this problem, we are developing a feedback system with a large loop-gain only in the vicinity of the frequencies $nf_{\rm rev} + f_{\rm s}$. They are the upper synchrotron sidebands of the revolution harmonics, and are responsible for driving the coupled-bunch oscillations. This feedback is realized by using a comb-filter comprising of an array of resonators. Each resonator is tuned to a particular frequency of $nf_{\rm rev} + f_{\rm s}$, and its phase is shifted properly to compensate for the phase differences among the sideband frequencies. The comb-filter can also compensate for the frequency-dependent amplitude response of the feedback loop by adjusting the attenuation of the resonators. The array of resonators is, from here on, referred to as the parallel comb-filter. A block diagram of the RF cavity feedback system is shown in Figure 8.39.

R&D Status

We have carried out a preliminary experiment of the parallel comb-filter feedback through the RF cavity. Figure 8.40 shows the experimental setup, which includes a parallel comb-filter, a 2-cell damped cavity of the Palmer type and a klystron. Since the cavity used was a cold model, only a small portion of the klystron output power was extracted with a 55dB directional coupler, to be fed into the cavity. The parallel comb-filter consists of five individual LC resonators arranged at 100 kHz intervals, and each resonator has a 2 kHz 3dB-bandwidth. A network analyzer was used to measure the amplitude and phase of the cavity voltage over the frequency range from 508 MHz

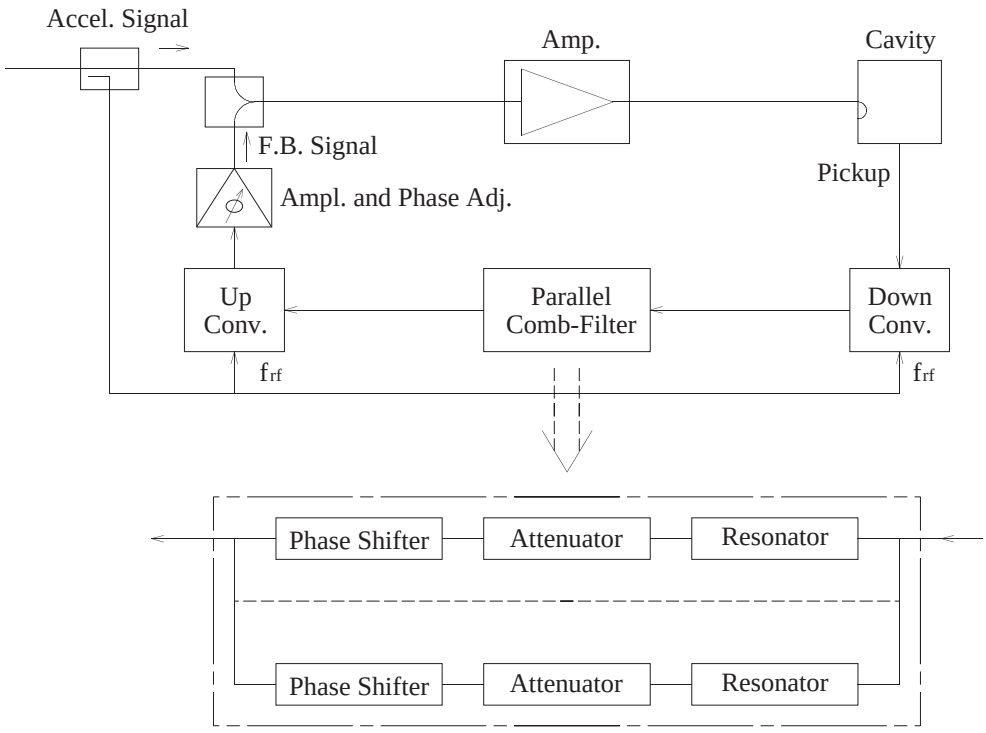

Figure 8.39: Block diagram of the RF cavity feedback system using a parallel comb-filter.

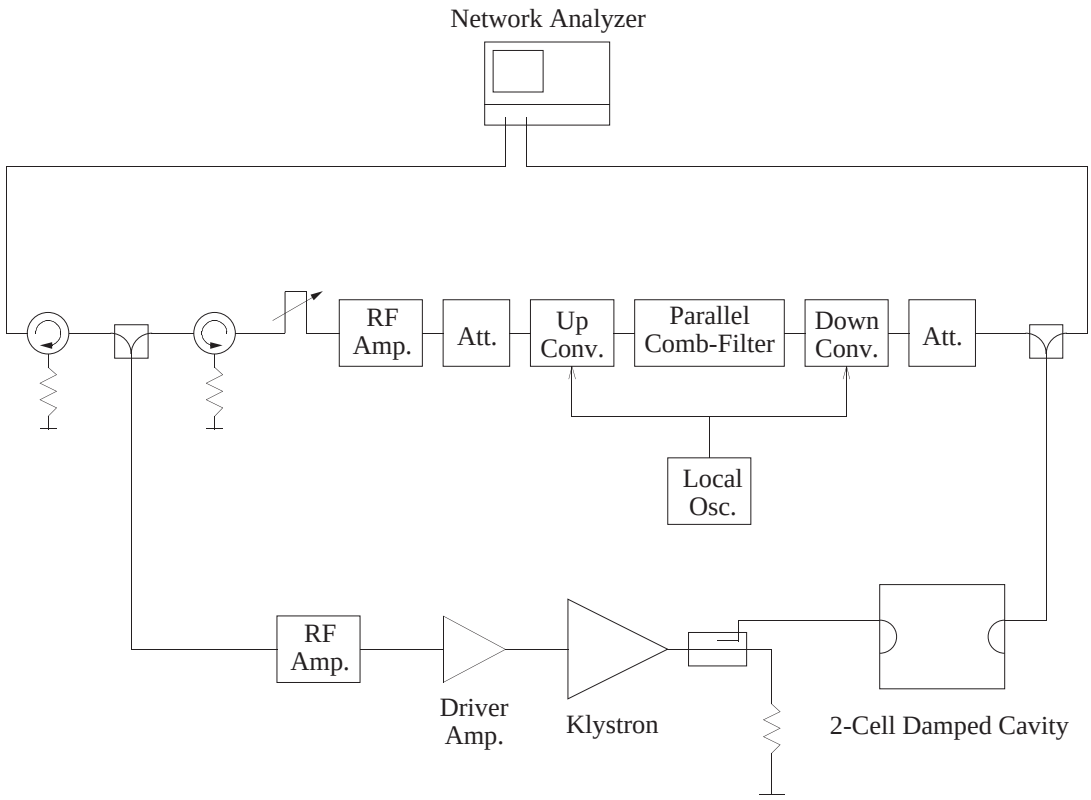

Figure 8.40: Block diagram of the experimental RF cavity feedback loop, which includes a parallel comb-filter, a low-power damped cavity and a klystron.

to 509 MHz. The bandwidth and the center frequency of the cavity were 236 kHz and 508.5 MHz, respectively.

The results of the measurement are shown in Figure 8.41; the top figure shows the magnitude and the real part of the effective cavity impedance, with or without feedback, as a function of the normalized frequency $(f - f_{\mathrm{rf}})/f_{\mathrm{rev}}$, and the bottom figure shows the phase of the cavity. With the feedback, the real part of the impedance was reduced by 17 dB to 25 dB, at five sideband frequencies. The measured values are in good agreement with estimations obtained by using the measured parameters of loop the components. The maximum gain of the feedback loop is limited by the top-to-bottom amplitude ratio of the filter, because the loop gain must be less than 0 dB at the bottom where the filter becomes 180° out of phase. The increase in the impedance between the revolution harmonics in Figure 8.41 is the result of a positive feedback due to an improper phase relationship in this region. An estimate shows that to reduce the real part of the cavity impedance by more than 35 dB, the 3dB-bandwidth of the resonator needs to be smaller than 1 kHz.

A new comb-filter with ten parallel resonators is currently being built. The center frequency of the resonator can be adjusted continuously and the bandwidth in a step-

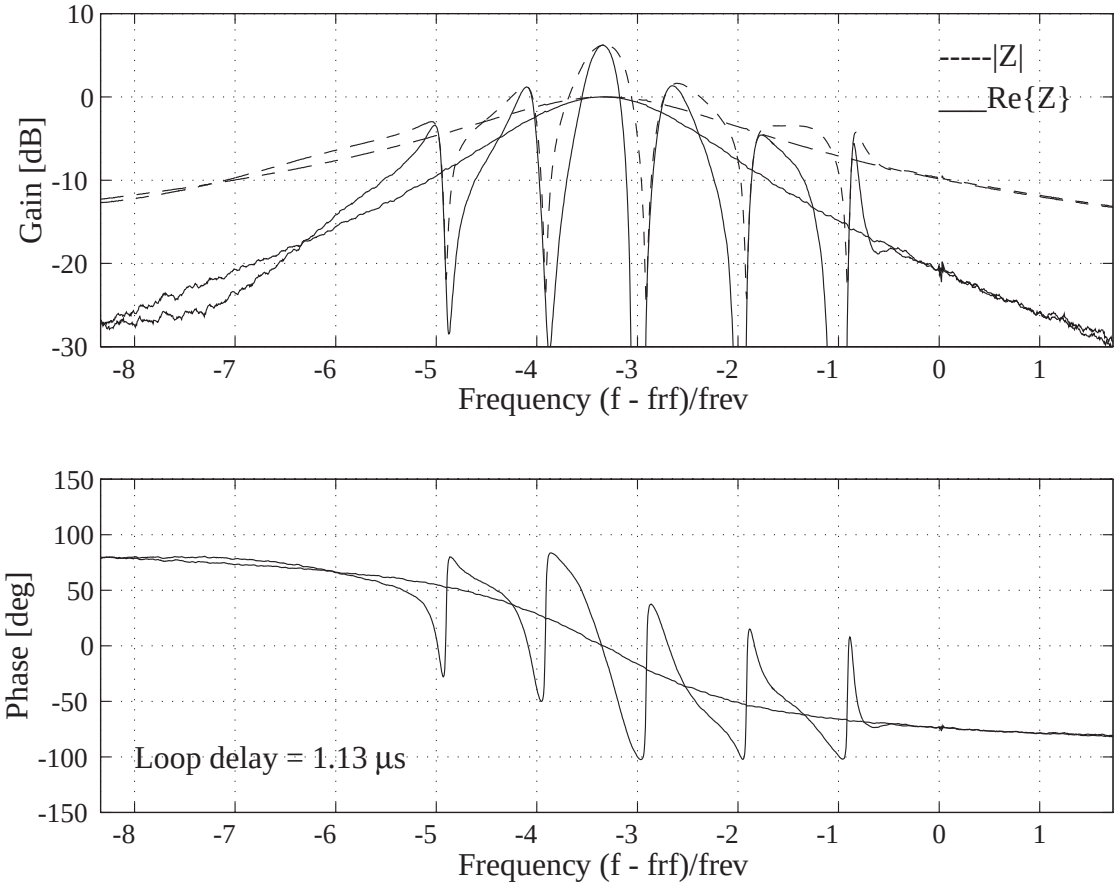

Figure 8.41: The results of the RF cavity feedback experiment. The top figure shows the magnitude and real part of the effective cavity impedance, with or without feedback, as a function of the normalized frequency $(f - f_{\rm rf})/f_{\rm rev}$; the bottom figure shows the phase of the cavity.

wise manner. The new comb-filter will be tested soon. The main purpose of the test is to improve the loop gain by more than 10dB. The RF cavity feedback system will be tested using a beam of the TRISTAN Main Ring (scheduled in May 1995).

8.4 Crab Cavity

8.4.1 Introduction

A large number of buckets in each ring (the HER and LER) must be filled with beams to obtain the design luminosity of 10^{34} /cm^{2}sec. Consequently KEKB has to operate with a short bunch spacing of minimum 60 cm. It is necessary, therefore, to separate both beams quickly near the interaction point (IP) to avoid parasitic collisions. It is also necessary to minimize synchrotron radiation generated near the IP, particularly just upstream of the crossing point. In order to meet these requirements, the interaction region (IR) design of KEKB is based on beam crossing with a finite angle of ± 11 mrad.

One consequence of employing a finite crossing angle is a luminosity reduction due to geometrical effects. Another important effect of a finite crossing angle is the possibility to excite synchrotron-betatron resonances. The crab crossing scheme [26], [27] is considered to solve these problems. Figure 8.42 shows the crab crossing scheme, where bunches are tilted by a time-dependent transverse kick in an RF deflector (crab cavity) located before the IP in each ring. After the bunches collide head-on, this bunch tilt is kicked back to the original orientation in another deflector after the IP.

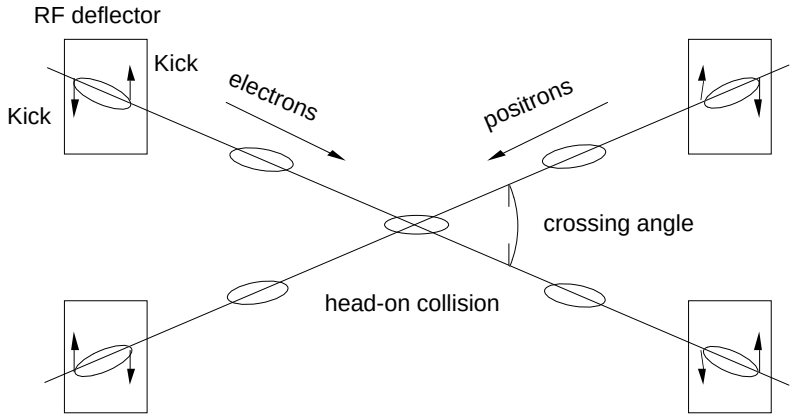

Figure 8.42: crab crossing scheme.

The R&D work on the crab cavity was carried out in 1991 and 1992 in collaboration with Cornell university, where superconducting crab cavities operating in the TM110 mode were designed for CESR-B at Cornell. In order to damp the parasitic modes, a new damping scheme that employs a coaxial beam pipe and a notch filter was proposed [5]. The damping scheme was verified by measurements of model cavities made of copper and aluminum. The high field performance was tested with a one-third scale niobium cavity in liquid helium. A cold measurement showed that the design values of

the necessary kick voltage and Q-value were achieved.

At KEK we started an R&D effort for the crab cavity aimed at making full-scale niobium cavities for KEKB in three years. We decided to adopt the same design of the crab cavity as that designed for CESR-B, although a slight modification is needed, since the frequency of KEKB is 508.9 MHz, which is slightly higher than that of CESR-B (500 MHz). In this section we describe the design and measurement results of the crab cavity that has been developed under the KEK-Cornell collaboration [5], [28]. At the end of this section our R&D plan for the crab cavity at KEK is presented.

8.4.2 Design Concept

Deflecting Mode

The required transverse deflecting voltage ($V_\perp$) is determined by the desired crossing angle at the IP and the operating frequency of the crab cavity:

$$V_\perp = \frac{cE \tan\theta_x}{\omega_{RF}\sqrt{\beta_x^* \beta_{crab}}}, \tag{8.1}$$

where β_x^*, β_{crab}, E, θ_x and ω_{RF} are the beta-function at the IP, the beta-function at the crab cavity, the beam energy, the half crossing angle and the RF frequency of the crab cavity, respectively. Table 8.11 summarizes the basic parameters for the crab cavities in the LER and the HER of KEKB. The required deflecting voltage is 1.4 MV in each ring.

One possible method to realize the crab crossing scheme is to use RF cavities operating in a transverse deflecting mode. The best choice for this would be the TM110 mode, which has a high transverse shunt impedance. Since superconducting

Table 8.11: Parameters for the Crab Cavity in KEKB.

Ring	LER	HER	
Beam energy	3.5	8.0	GeV
RF frequency	508.887		MHz
Crossing angle	±11		mrad
β_x^*	0.33	0.33	m
β_{crab}	20	100	m
Required kick	1.41	1.44	MV

cavities can be operated in a high field gradient, a single-cell superconducting cavity would be sufficient to provide the necessary transverse kick voltage.

Damping Scheme for Parasitic Modes

Coupled-bunch instabilities caused by the crab cavities must be sufficiently suppressed, as well as those caused by the accelerating cavities of KEKB. The Q-values of dangerous parasitic modes should be sufficiently lowered, typically to the order of 100. In the case of superconducting accelerating cavities, the accelerating mode is the lowest frequency mode, and all parasitic modes have higher frequencies. As a damping scheme for higher order modes, the superconducting accelerating cavity for KEKB employs large-diameter beam pipes, through which the field energy of those modes can be extracted and absorbed by microwave absorbers attached to the beam pipe.

In the case of a crab cavity, however, since the operating mode (TM110) used for the crabbing is not the lowest frequency mode, there are some modes with lower, or about the same, frequencies. Four unwanted parasitic modes remain trapped in the cavity region with high Q-values, even if a beam pipe with a large diameter is attached. Those are the TM010 monopole mode, two polarizations of the TE111 dipole mode and an unwanted polarization of the TM110 mode. In order to overcome this problem, a coaxial beam pipe and a notch filter are employed in the crab cavity. A schematic view of this damping scheme is shown in Figure 8.43. With this scheme, not only the higher order parasitic modes, but also the lower frequency parasitic modes, can be damped, as will be discussed in the following.

In a coaxial transmission line, although there is no cut-off frequency for TEM mode waves, there is a cut-off frequency for the dipole modes. By attaching a coaxial beam

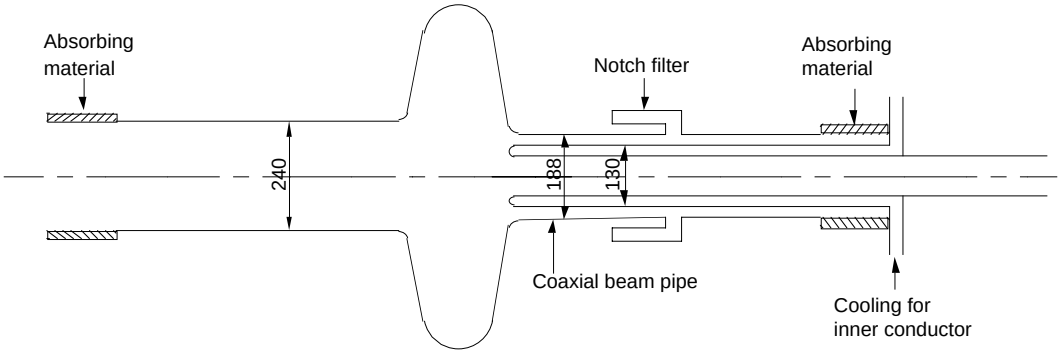

Figure 8.43: A schematic view of the crab cavity.

pipe to the crab cavity, every monopole resonant mode in the cavity can couple to the coaxial beam pipe as a TEM mode wave, and then propagate. In addition, every dipole resonant mode in the cavity can couple to the coaxial beam pipe as a dipole mode wave; it will propagate if its frequency is higher than the cut-off value. By designing a cell shape such that f(TM110)$<$ f(cut off)$<$ f(TE111), all monopole and dipole modes, except the TM110 mode, in the cavity can be extracted out of the cavity via the coaxial beam pipe.

However, one unwanted polarization of the TM110 mode is still trapped in the cavity. Since this mode has a high transverse shunt impedance, it must be cured. Two possible measures for cure have been considered:

- Use of a slightly polarized cell, and tuning this mode at a safe frequency. If we control the frequency of this mode at a damping side of transverse coupled-bunch instability, we can avoid the instability driven by this mode. For this method we designed a round cell shape cavity using cylindrical symmetric calculations. A slight polarization will be introduced to separate the unwanted polarization mode from the operating mode.

- Extremely polarized cell ("Squashed" crab cavity). By making the cross section of the cavity cell an ellipse or race-track shape with a large eccentricity, we can increase the frequency of the unwanted TM110 mode to be above the cut-off of the dipole mode wave in the coaxial beam pipe. An analytical calculation of a rectangular cavity has shown that when the ratio of the longer to shorter dimension in the cross section is 2:1, the unwanted TM110 mode goes up to 700 MHz, while the operating mode is kept at 500 MHz. We designed such an extremely polarized cell cavity.

In the following we describe both designs of the round cell and the squashed cell.

8.4.3 Design Optimization

Coaxial beam pipe

Since we will operate the crabbing mode TM110, at 509 MHz, the cut-off frequency of the dipole mode in the coaxial beam pipe should be higher than that frequency. In order to have a sufficient attenuation for the crabbing mode, it is desirable to make the cut-off frequency high enough. On the other hand, the cut-off frequency should be lower than the lowest parasitic dipole mode (TE111 in this case). The dimensions of the coaxial beam pipe were chosen so that: (1) it has a cut-off frequency of 600 MHz, which gives an attenuation of 60 dB/m for the crabbing mode, and (2) it has a sufficient

thickness of the inner conductor to allow a cooling system in it. We have chosen the radius of the inner surface of the outer pipe to be 94 mm and the outer and inner radii of the inner conductor to be 65 mm and 45 mm, respectively.

Round cell design

Computer studies involving a cylindrical symmetry have been carried out in order to optimize the cell shape. The variables in the optimization were the cell length, the iris radius, the equator radius and the slope of the wall. Several points taken into account in designing the cell shape were:

- The frequencies of all dipole parasitic modes should be higher than the cut-off frequency of the dipole mode in the coaxial beam pipe.
- The ratio of the kick voltage to the surface peak field should be high.
- The R/Q values of the parasitic modes (especially for the most dangerous TM010 mode) should be low.
- The external Q for parasitic modes having high R/Q should be low (typically less than on the order of 100).

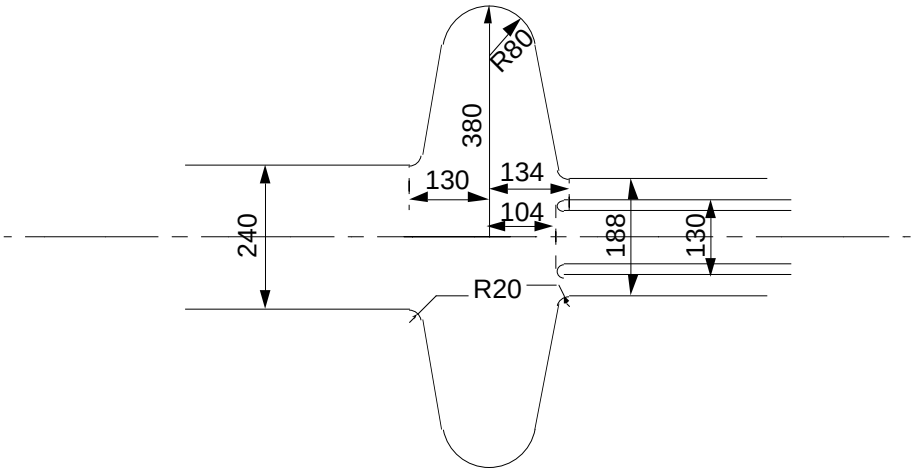

Figure 8.44: Cell shape of the round crab cavity.

The kick voltage, surface field, frequency and the R/Q value were calculated by using URMEL. The external Q-values were calculated with URMEL by changing the short position of the beam pipe by using Slater's formula [22]. The external Q-values for monopole modes were also calculated using SEAFISH by assuming a ferrite absorber

Table 8.12: RF properties of the round cell crab cavity.

Crabbing Mode (TM110)					
Frequency	500	(MHz)			
$R*/Q$	51.2	Ω/cell			
Kick voltage	(MV)	2.0	at E_{sp}=21.7 MV/m, H_{sp}=750 Oe		
Loss factor	(V/pC)	0.58			
Parasitic modes					
mode	frequency (MHz)	R/Q (Ω/cell)	Q_{ext} coax	Q_{ext} hollow	Q_{loaded} total
(Monopole modes)					
TM010	342	135	108	-	108
TM020	731	26	40	-	40
TM011	914	21	38	-	38
TM030	1107	1	141	165	76
TM021	$\sim$1200	4	$<$100	$<$100	$<$100
(Dipole modes)					
TE111	720	6	18	-	18
TM120	898	6	160	37	30
TE112	1048	1	$\sim$1000	186	$\sim$161
TE121	$\sim$1100			$<$100	$<$100

$R/Q = (V(r_0)^2/\omega U)/(kr_0)^{2m}$, where m=0 (monopole) and m=1 (dipole).
E_{sp} and H_{sp} is the surface peak electric and magnetic field, respectively.

attached to the beam pipe. The loss factor was calculated using TBCI. Figure 8.44 and Table 8.12 show the cell shape and RF properties of the final design. The Q-values of dangerous (high R/Q) monopole and dipole parasitic modes are damped to less than 100 with the coaxial beam pipe.

Squashed cell design

The design of the extremely polarized cell (squashed cell) was carried out by using MAFIA. In addition to the considerations taken in the round cell design, the frequency of the unwanted polarization of the TM110 mode was increased up to 700 MHz so that it propagates in the coaxial beam pipe. Figure 8.45 and Table 8.13 show the cell shape and RF properties of the final design. The Q-values of dangerous (high R/Q) monopole and dipole parasitic modes are damped to less than 100 with the coaxial beam pipe, similarly as for the round cell case.

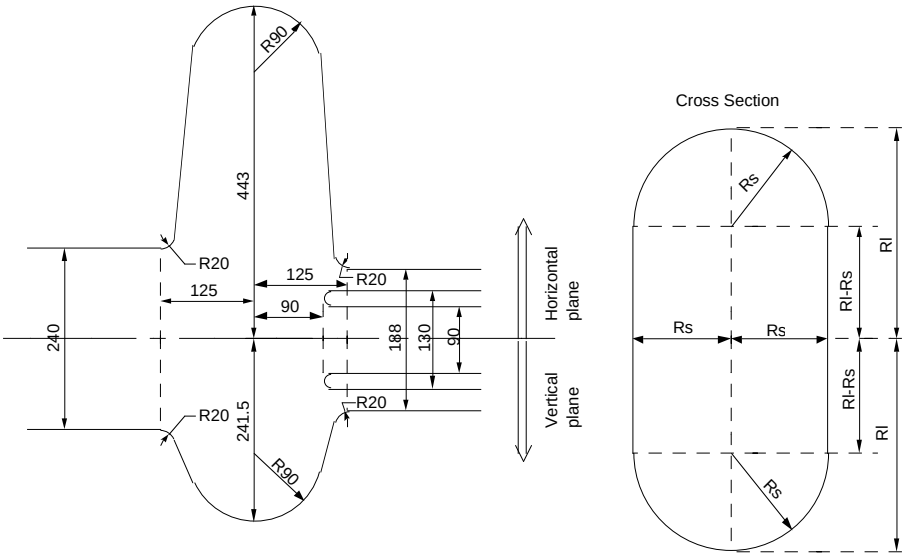

Figure 8.45: Cell shape of the squashed crab cavity. In the left side figure, the upper part shows the cross section in the horizontal plane, while the lower part shows that in the vertical plane.

Notch filter

Since the crabbing mode is a dipole mode and its frequency is below the cut-off of the coaxial beam pipe, the crabbing mode attenuates in the coaxial beam pipe. With our design, the crabbing mode is sufficiently attenuated and the power dissipation

Table 8.13: RF properties of the squashed cavity.

Crabbing mode							
Frequency	(MHz)	501.7					
$R*/Q$	(Ω/cell)	47.2					
Kick voltage	(MV)	2.0	at Esp=24.6 MV/m				
Parasitic modes							
MAFIA calculation						Model measurement	
mode	Frequency	R/Q	Q_{ext}	Q_{ext}	Q_{loaded}	Frequency	Q_{loaded}
*x-y-z	(MHz)	(Ω/cell)	coax	hollow	total	(MHz)	w/ferrite
[Monopole-like parasitic modes]							
TM1-1-0	413.3	99.8	96	-	96	415.0	123
TM3-1-0	670.6	17.3	76	-	76	672.6	50
TM1-1-1	946.6	9.9	118	-	118	938.6	$\sim$130
TM5-1-0	967.2	0.08	358	1273	279	966.2	$\sim$130
TM1-3-0	992.3	$\sim$2.2		379	$<$379	1000.1	$\sim$130
[Dipole-like parasitic modes]							
TE1-0-1	650.6	10.0	149	-	149	641.2	66
TE0-1-1	677.6	5.9	46	-	46	666.4	50
TM1-2-0†	686.5	23.0	37	-	37	686.5	22
TM4-1-0	792.9	8.1	97	99	49	789.4	70
TM3-2-0	870.0	1.1	161	56	42	891.0	60
TE3-0-1	964.1	1.2	144	63	44	936.1	$<$60
TM2-1-1	1024.9	1.2	29000	1414	1350		$<$350
TM2-3-0	1044.1	0.13	74000	578	574		$<$350
TE1-2-1	1095.7	0.28	$>$1000	82	82		

**Each mode number is identified by a rectangular coordinate system instead of a cylindrical coordinate system.

† – This mode is the unwanted polarization of the crabbing mode.

$R/Q = (V(r_0)^2/\omega U)/(kr_0)^{2m}$, where m=0 (monopole) and m=1 (dipole).

E_{sp} and H_{sp} is the surface peak electric and magnetic field, respectively.

For the convenience of comparison, the numbers quoted as the "model measurement frequency" are the actual frequency divided by three. This is because the module used in the test is a one-third scale test model.

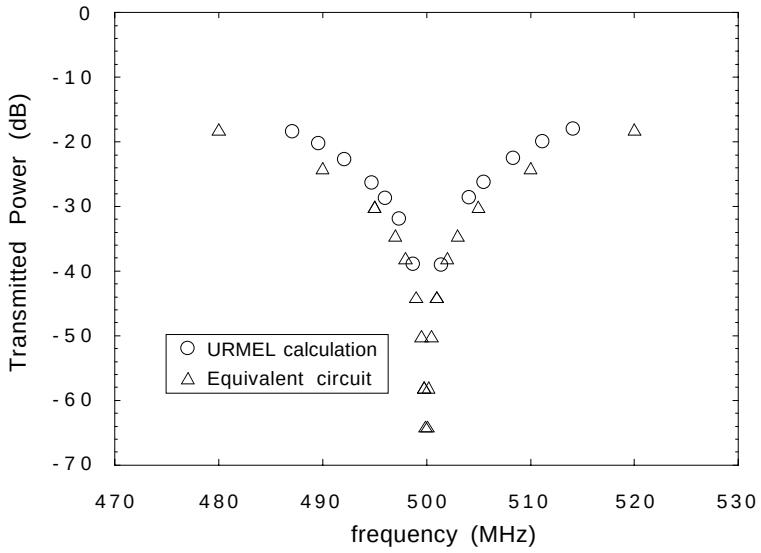

Figure 8.46: Frequency characteristics of the notch filter.

caused by this mode in the ferrite absorber at the end of the coaxial beam pipe is less than 1 kW. In a real cavity, however, some asymmetry due to machining errors or a misalignment of the coaxial beam pipe can transfer a part of the field energy of the crabbing mode into a TEM mode wave in the coaxial beam pipe. This TEM wave propagates down the coaxial beam pipe without attenuation, resulting in an increase of the dissipation power at the ferrite absorber. In order to avoid this, we have attached a notch filter which rejects the TEM-coupled crabbing mode back to the cavity.

Figure 8.46 shows the transmission property of the notch filter calculated using URMEL, together with the results of an analytical calculation of an equivalent circuit. If the resonant frequency of the filter is tuned within ± 0.5 MHz, a rejection rate higher than 50 dB is obtained. Even if the external Q for the crabbing mode might be reduced to 10^5 for a machining error or misalignment, this rejection of 50 dB assures an external Q of 10^{10}, which is sufficiently high.

The resonant frequency of the filter can be tuned by changing the filter iris. According to SUPERFISH calculations, the rate of the frequency shift is 1.8$\sim$3.6 MHz/mm.

In addition to the stopband at 500 MHz, the notch filter has a higher order TEM stopband at 1.45 GHz. Since there are several parasitic modes near this frequency, the hollow beam pipe opposite to the coaxial beam pipe has been opened wide enough so that the monopole modes above 1.3 GHz and the dipole modes above 1 GHz escape from the hollow beam pipe.

8.4.4 Model Measurements

In order to examine new ideas concerning the parasitic mode damping, we have built a one-third scale (L-band) round copper cavity and a one-third scale squashed aluminum cavity, with a coaxial beam pipe and ferrite absorbers. In addition, a high field performance test was made in liquid helium with a one-third scale round cell niobium cavity equipped with a coaxial beam pipe and a notch filter made of niobium.

Coaxial Beam Pipe Measurement

First, we measured the effect of the coaxial beam pipe on the damping property of the TM010 monopole mode, and on the Q-value of the crabbing mode. Figure 8.47 shows the loaded Q-value of the TM010 mode as a function of the penetration length of the inner conductor of the coaxial beam pipe into the cavity cell. The Q-value is damped below 100 with moderate penetration. The result agrees with a SEAFISH calculation within a factor of two.

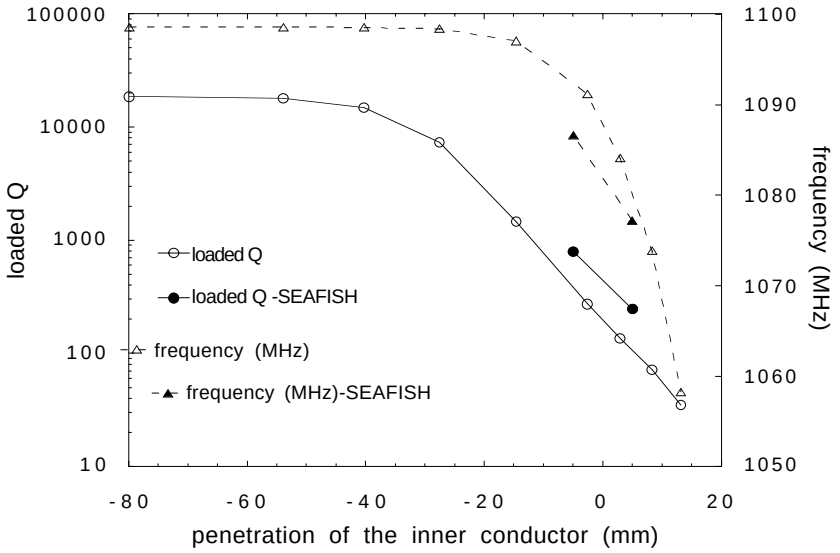

Figure 8.47: Damping of the TM010 mode in the crab cavity with a coaxial beam pipe.

Figure 8.48 shows how a misalignment of the inner conductor relative to the outer conductor affects the crabbing mode. When the inner conductor is aligned within 1 mm, the loaded Q-value with and without the coaxial beam pipe are nearly the same. Since the intrinsic Q of this copper cavity is 23000, this means that the external Q of the coaxial beam pipe, when thus-aligned, is at least on the order of 10^5. As mentioned earlier, the notch filter assures an additional 50 dB reduction, which makes

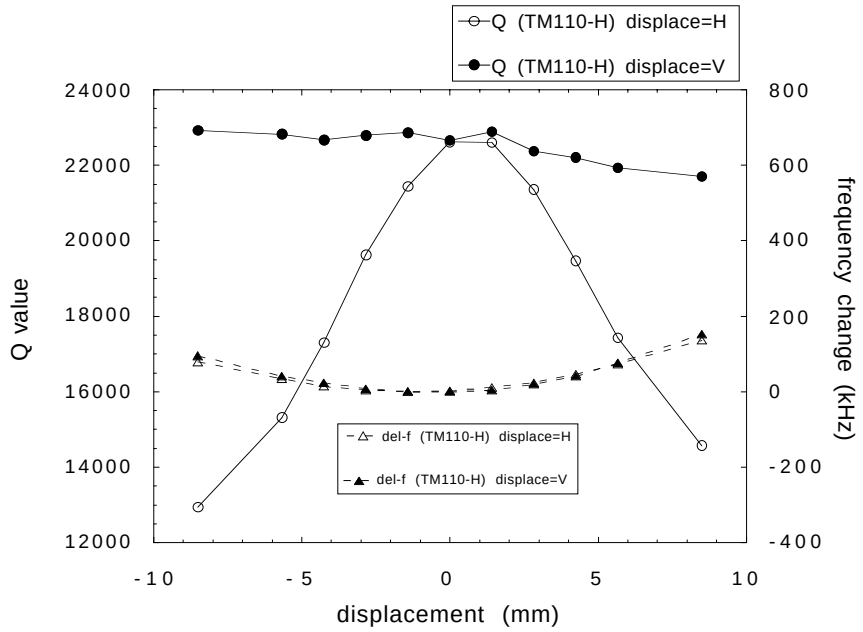

Figure 8.48: Effect of misalignment of the coaxial beam pipe on the crabbing mode.

the external Q-value above 10^{10}. Different sensitivities of the Q-values with respect to the horizontal and vertical displacements are considered to be due to the fact that the electric field at the tip of the coaxial beam pipe is polarized horizontally. Since this is a result of the one-third scale model, the alignment tolerance for the full-scale cavity is expected to be about 3 mm, which can be easily achieved.

Squashed Cavity Model Measurement

The resonant frequency and the damping properties have been measured with the one-third scale squashed crab cavity. Figure 8.49 shows the frequency spectrum with and without the coaxial beam pipe and ferrite absorbers. The measured frequency of each mode and the Q-values with the ferrite absorbers are listed in Table 8.13 together with the results of MAFIA calculations. As expected from the MAFIA calculation, all the dangerous monopole and dipole modes are damped to less than on the order of 100, including the unwanted polarization of the crabbing mode. A high Q-value is maintained for the crabbing mode. The external Q-value of the crabbing mode via the coaxial beam pipe was estimated from the measured loaded Q-value with and without the coaxial beam pipe. It has been estimated to be at least on the order of 10^5, which is the same result as in the case of a round-cell cavity.

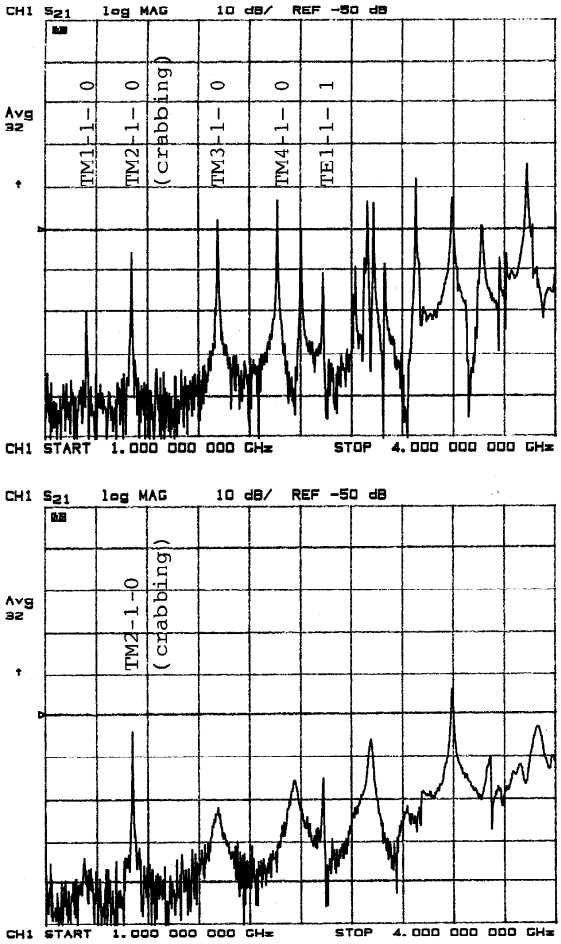

Figure 8.49: Frequency spectrum of a squashed crab cavity: (upper) without a coaxial beam pipe and (lower) with a coaxial beam pipe and a ferrite absorber.

High Field Performance

The kick voltage required for crabbing is 1.4 MV which corresponds to a surface peak field of 15 MV/m. According to the present technology of superconducting accelerating cavities at around 500 MHz, a surface peak field of 20 MV/m can be easily achieved, which corresponds to an accelerating gradient of about 10 MV/m . For the crab cavity, it is still crucial to confirm high field performances, because it has several new features, such as the coaxial beam pipe and the notch filter on the beam pipe, which might cause some limitation to the field due to multipactoring or other causes.

Figure 8.50 shows the one-third scale niobium cavity mounted on a test stand. Measurements of the TM110 mode at 1.5 GHz were made when the system was cooled down to 1.5 K in liquid helium. At a surface peak field of 1 MV/m a multipactoring was encountered, which is considered to have occurred at the coaxial beam pipe. The multipactoring was processed away after an hour of RF processing. Figure 8.51 shows the Q-value versus the surface peak field. The maximum surface peak field was 25 MV/m, where we experienced field emission. The kick voltage required for KEKB has been achieved with a sufficiently high Q-value. Thus, the feasibility of the crab cavity has been realistically demonstrated.

Figure 8.50: One-third scale Niobium round-cell crab cavity mounted on a test stand.

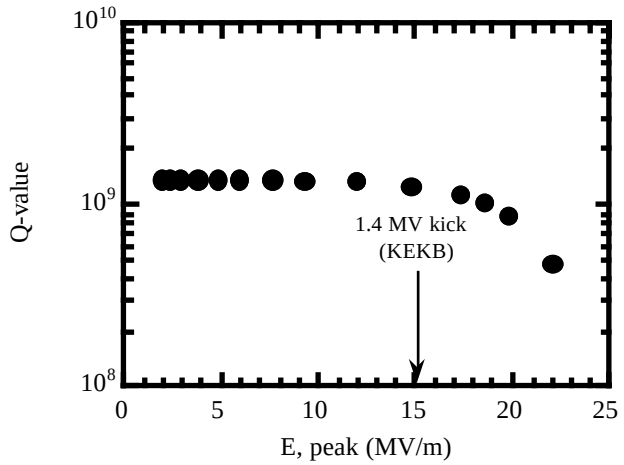

Figure 8.51: Surface peak field vs Q-value measured in liquid helium.

8.4.5 R&D Schedule

In the R&D program of the crab cavity at KEK, we are planning to fabricate full-scale superconducting cavities in three years. For the base line design of the crab cavity, we have adopted a squashed cell shape cavity scheme, which was designed and extensively studied at Cornell for CESR-B under the KEK-Cornell collaboration. The R&D work on the crab cavities at KEK will take advantage of the fabrication and measurement techniques of niobium superconducting cavities that have been established through constructing the TRISTAN SCRF system.

Figure 8.52 shows the R&D schedule of the crab cavity for KEKB. At the first stage of the R&D program, a test stand with a vertical cryostat and an RF measurement system for a one-third scale model will be completed by the end of JFY1994. The one-third scale round cell shape Nb cavity that has been designed, fabricated and tested at Cornell for CESR-B will be tested again at KEK. Three one-third scale squashed cell shape model cavities will be designed and built to establish the fabrication technique for a non-axially symmetric structure by the end of FY1995. At the final stage of the R&D, two full-scale squashed cell shape prototype cavities, equipped with coaxial beam pipe and notch filter, will be designed and fabricated. After an RF test in a vertical cryostat, one of these cavities will be installed in a horizontal cryostat. The prototype cavity in a horizontal cryostat will be cooled down by a helium refrigerator, and a high power RF test will be conducted to confirm the performances that are required for KEKB.

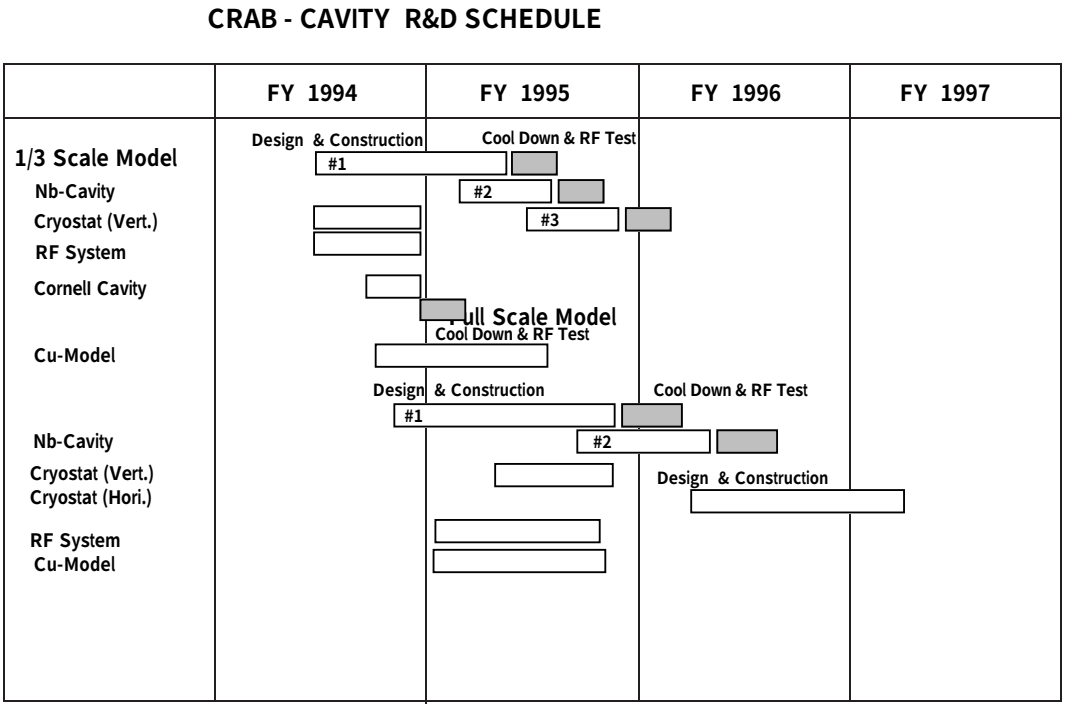

Figure 8.52: R&D schedule of the crab cavity at KEK.

Bibliography

[1] Y. Yamazaki and T. Kageyama, *Particle Accelerators* **44** 107 (1994).

[2] T. Shintake, *Particle Accelerators* **44** 131 (1994).

[3] K. Akai and Y. Yamazaki, *Particle Accelerators* **46** 197 (1994).

[4] Z. D. Farkas *et al.*, *Proc. 9th Int. Conf. on High Energy Accel.* , SLAC 576 (1974).

[5] K. Akai, J. Kirchgessner, D. Moffat, H. Padamsee, J. Sears, T. Stowe and M. Tigner, *Proc. B Factories* **SLAC-400** 181 Apr. 6-10 SLAC (1992), and *Proc. 15th Int. Conf. on High Energy Accel.* 757 (1992).

[6] T. Shintake, *Jpn. J. Appl. Phys.*, **31** L1567 (1992).

[7] HP Part No. 85180A., HP Corp.

[8] N. Akasaka, T. Kageyama and Y. Yamazaki, *Proc. 4th European Part. Accel. Conf.* , 2137 (1994).

[9] F. J. Sacherer, *IEEE Trans. Nucl. Sci.* **NS-20** 825 (1973).

[10] T. Kageyama, N. Akasaka, Y. Takeuchi and Y. Yamazaki, *Proc. 4th European Part. Accel. Conf.* , 2098 (1994).

[11] H. Matsumoto *et al.*, *Proc. 9th Linear Accelerator Meeting in Japan*, Kyoto, pp. 124-126 (1984).

[12] S. Isagawa, *et al.*, *Proc. IEEE Part. Accel. Conf.* , Washington, D.C., 1934 (1987).

[13] S. Yamaguti, *et al.*, *IEEE Trans. Nucl. Sci.* , **39, No. 2**, 278 (1992).

[14] M. Akemoto, KEK preprint 91-45 (1991).

[15] S. Mitsunobu, private communication.

[16] A. Ueno, *et al.*, KEK preprint 94-117 (1994).

[17] F. Naito, *et al.*, KEK preprint 90-99 (1990).

[18] F. Naito, *et al.*, KEK preprint 94-115 (1994).

[19] T. Weiland, DESY report 83-073, (1983).

[20] T. Takahashi *et al.*, *Proc. 9th Symposium on Accelerator Science and Technology*, KEK, 327 (1993).

[21] T. Kageyama, *Proc. 15th Linear Accelerator Meeting in Japan*, (1990).

[22] J. C. Slater, *Microwave Electronics*, Van Nostrand (1950).

[23] K. Asano *et al.*, submitted to the 1995 Part. Accel. Conf.

[24] T. Tajima *et al.*, *Proc. 6th Workshop on RF Superconductivity*, CEBAF, 962 (1993).

[25] K. Akai and E. Ezura, *Proc. 4th European Part. Accel. Conf.* , 1141 (1994).

[26] R. B. Palmer, SLAC-PUB 4707 (1988).

[27] K. Oide and K. Yokoya, *Phy. Rev.* **A40** 315 (1989).

[28] K. Akai, J. Kirchgessner, D. Moffat, H. Padamsee, J. Sears and M. Tigner, *Proc. IEEE Part. Accel. Conf.* (1993).